Master thesis and internship[BR]- Master's thesis : Development of a Coupling Interface Between a High Order Discontinuous Galerkin Method and External Structural Solvers for Gas Foil Bearing Analysis[BR]- Integration Internship : Mitis

Auteur : Agnello, Hugo
Promoteur(s) : Hillewaert, Koen
Faculté : Faculté des Sciences appliquées
Diplôme : Master en ingénieur civil en aérospatiale, à finalité spécialisée en "aerospace engineering"
Année académique : 2022-2023
URI/URL : http://hdl.handle.net/2268.2/18151

Development of a Coupling Interface Between a High Order Discontinuous Galerkin Method and External Structural Solvers for Gas Foil Bearing Analysis

Master's thesis completed in order to obtain the degree of Master of Science in Aerospace Engineering

HUGO AGNELLO

Advisor:
Prof. Koen Hillewaert - ULiège

Committee members:
Prof. Romain Boman - ULiège
Prof. Loïc Salles - ULiège
Dr. Michel Delanaye - MITIS

University of Liège - School of Engineering and Computer Science
Academic year 2022-2023

Acknowledgments

I would like to express my sincere thanks to all the people who have helped me in the accomplishment of this work.

First of all, I would like to thank my supervisor Prof. Koen Hillewaert for his guidance, his help and his involvement in my work.

I would also like to thank Martin Heylen, Michel Delanaye and all the employees of Mitis SA for their welcoming and goodwill towards me during my internship.

Likewise, I would like to thank the University's ForDGe team for their help and advice when I needed them and particularly Nayan and Amaury.

Thank you to Adrien, Louis and Valentin and to all my friends who have accompanied and supported me throughout the last five years and more.

Last but not least, I would like to thank my family for their support and Charline for her proofreading and encouragement throughout the accomplishment of this master's thesis and much more.

Abstract

This master's thesis purpose is to develop a coupling interface between a high-order aerodynamic solver and external structural solvers. Firstly, an actualised state-of-the-art of the foil bearing technology and its modelling methods is provided to justify the necessity of such an interface. The implementation of the latter is presented and validated through a comparative analysis between internal and external structural solvers for multiple test cases. The impact of the externalisation process has been evaluated for different structural solvers and a beam finite element method has been implemented to analyse the effects of top foil modelling on the overall gas foil bearing behaviour.

The development of this interface opens up a lot of possibilities for further analysis and coupling with higher complexity and/or high-order structural solvers, some of which are presented in this report.

Contents

Chapter 1

Introduction

1.1 Context

Gas foil bearings (GFBs) are a type of hydrodynamic fluid bearing which uses gas as a working fluid to separate a rotating shaft from the bearing by a thin film of gas.

Such bearing's advantages lie in the fact that, once the formation of the gas film has been achieved, no more wear occurs between the journal and the bearing. It assures contamination-free operation of the working fluid and it can help reduce noise or be used in noise-sensitive operations. Moreover, GFBs are oil-free and self-cooling bearings. They do not require as much maintenance as their counterparts and can also be lighter.

As GFBs can create this hydrodynamic gas film without any outside assistance, their specific properties above-mentioned make this type of bearing very attractive for many industrial applications, especially in the turbomachinery domain [1]. GFBs have been investigated for applications in turbochargers/turbojets [2, 3, 4], turbofan engines [5], micro gas turbine engines [6, 7], and much more. The GFB's capacity to sustain very high rotation speeds and broad power range makes it particularly suitable for micro-small high-power density turbo machinery [8].

However, these advantages come with high design and manufacturing complexity. As a result, a lot of ongoing research is trying to exploit this promising technology [9]. This research focuses as much on the numerical modelling side as on the experimental side, to predict the behaviour and deepen the understanding of the gas foil bearing technology for different kinds of applications in air-cycle machines and high-speed machinery.

1.2 Working Principle

All gas foil bearings rely on the same principles and present the same major components: on one hand, the bearing casing, which is also named the sleeve, is the rigid external part of the bearing holding the journal in position and, on the other hand, the compliant component lies in between the sleeve and the journal. Even though this compliant part of the bearing can take many different forms, it is often made from the coupling of a bump-type foil, which generates most of the stiffness and the damping, with a smooth foil on top of it, i.e. the top foil.

At the start-up, the journal and the top foil are in contact, and the rotation of the shaft will start drawing in the ambient gas, which is often the air, in the bearing via viscosity effects. Then, once the liftoff rotation speed of the bearing is reached, this hydrodynamic gas film will be fully developed and will act as a lubricant between the rotor and the bearing. This will push back the top foil. At this point, there is no more contact between the bearing and the journal and no more wear occurs, until the halt of the rotative machine and thus the journal's rotation.

A perturbation to the system, which would cause a journal misalignment, increases locally the pressure in the hydrodynamic gas film and pushes the journal back into its nominal place. The bearing acts as a controller and provides stiffness and damping to the system.

1.3 Objectives and Motivations

The main goal of this master's thesis is the implementation of a method that allows ForDGe to be coupled with an external structural solver. ForDGe is the high-order aerodynamic solver that is going to be presented in section 3.1. The objective of this implementation is to be able to represent with high accuracy the coupling of the aerodynamic forces with the elastic forces present in a working gas foil bearing. The structural model would compute the stiffness and the deformation of the compliant foils under a pressure field computed by ForDGe.

Many different structural models representing the compliance of the foils exist for varying computation performance and physical accuracy. To achieve this coupling in an efficient way, ForDGe must be adapted to be able to receive an external field as input, which would represent the gap between the top foil and the journal. This external gap could be computed and delivered to ForDGe by any relevant structural model of the compliant structure. This would enable ForDGe to receive and use data from any mesh type and any order of interpolation and to use it as an input parameter.

The purpose of this work is thus to open the way to high-accuracy analysis of different gas foil bearing configurations or parameters by coupling high-order aerodynamic and structural solvers.

1.4 Outline of the Thesis

This report is divided into five chapters. In the first chapter, the work and its objectives are introduced. A brief explanation of the functioning of gas foil bearings is also provided. In the second chapter, a literature review of the gas foil bearing technology, specifically on the different GFB configurations and the modelling techniques is established. Chapter three presents the numerical methodology implemented in the frame of this work and the inner workings of the iterative process between solvers. It also presents some mathematical

principles of the discontinuous Galerkin finite element method, which is the basis of ForDGe. The fourth chapter shows the results and contains their analysis as well as the validation of the implemented numerical coupling. Finally, chapter five concludes this master's thesis and presents some potential future use of the implemented method for further analysis.

Chapter 2

Literature Review

Many different types of gas foil bearings exist, and several different numerical models have been used to characterise them. No scientific consensus has been reached to establish what bearing type or numerical model of foil structure is the best or the most well suited to reach the high precision required for static models as well as dynamic ones. The following tries to compile and provide a recent and updated review of the state-of-the-art of different GFB types and modelling methods.

2.1 Different Configurations of Gas Foil Bearings

Even though many different configurations and variations of GFBs exist, only two different bearing types will be extensively reviewed in this work, as they are those being investigated by Mitis SA. However, the implementation allows for any structural solver to be coupled with ForDGe. Therefore, any gas foil bearing type could be analysed with the same method, as long as the bearing's parameters are well defined or well known. Such bearing will be briefly presented in subsubsection 2.1.1.3. The main category of bearings that will be reviewed is "journal gas foil bearings". Thrust bearings are only briefly mentioned, as they are outside the scope of this work, but could be analysed by this method under a few modifications.

2.1.1 Journal Gas Foil Bearings

2.1.1.1 Bump Foil Type Bearing

Bump foil bearings, represented in Figure 2.1, get their compliance from a coupling of a bump foil with another foil laying on top of it, namely the top foil. At nominal speed, once the film gas between the journal and the top foil is fully developed, the pressure will maintain the journal and the foil apart. Increasing eccentricities e during operation due to various parameters, such as vibrations or response to an external excitation, will reduce the gap h. However, this will also increase the pressure in the gas film and thus push back the compliant coupling of the bump and top foil.

These kinds of bearings present some advantages that could be of potential use to the industry, such as weight reduction from the absence of any oil system, as gas foil bearings can work with the ambient air and stability at higher working speeds and temperatures [10, 11]. The application of gas foil bearings leads to less dependency on other components or subsystems such as cooling systems, lubrication systems, pumps, etc., which reduces maintenance costs and complexity. Nonetheless, at low rotation speeds, GFBs have a lower load capacity, as well as modest stiffness and damping values [12].

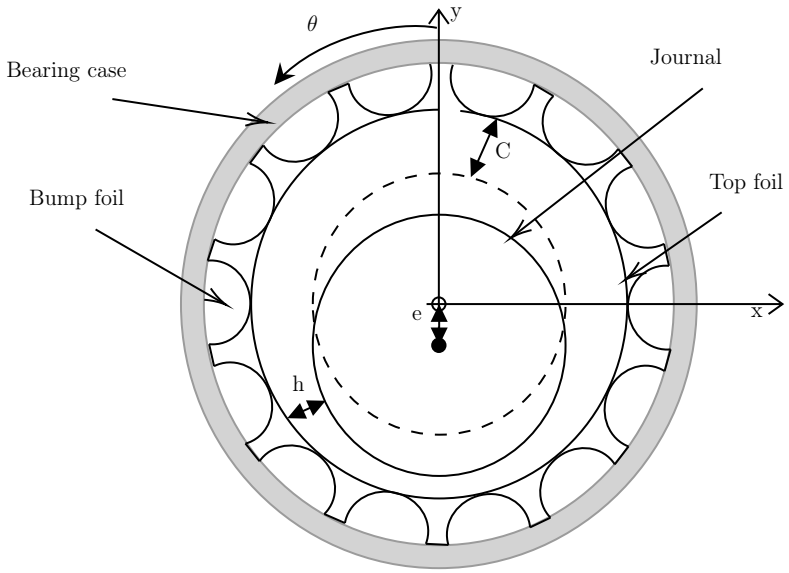

Figure 2.1: Bump gas foil bearing with a single 360° pad.

Bump configuration type bearings can vary by their number of pads. In Figure 2.1, only one full 360° pad is shown. However, the three 120° pads configuration represented in Figure 2.2 is frequently used in scientific and industrial research for this type of GFBs as well as for other bearing types.

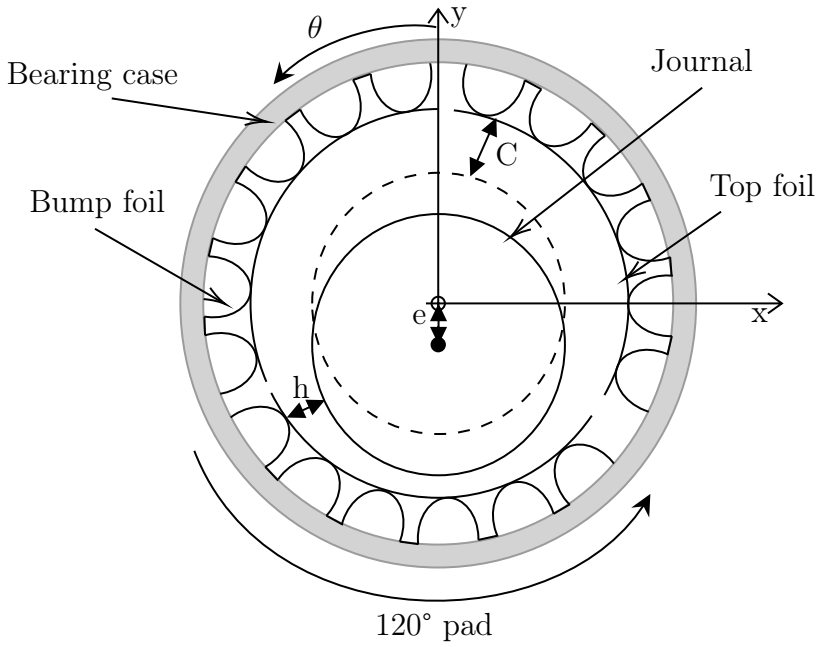

Figure 2.2: Bump gas foil bearing with three 120° pads.

Gas foil bearings with more than one bump foil have also been studied and are called multi-decked. As suggested by Heshmat [13], a multi-decked bump type bearing with additional bump foils leads to an increase in non-linear stiffness. They were studied by Yu et al. [14] and by Lai et al. [15].

Xu et al. [16] also studied multi-decked GFBs and presented a structural model for performance analysis of such bearings. They also showed that compared to a simple bump GFB:

- a multi-decked GFB with a stiffer bump foil could generate a more evenly distributed gas film for an equivalent loading,
- a multi-decked GFB with a softer bump foil could have better load capacity and overall stiffness.

However, it is good to note that a multi-decked GFB's performances rely heavily on the foils' layout and adjustments.

2.1.1.2 Cantilever Foil Bearing

Cantilever foil bearings don't have a classic bump foil, the latter being replaced by an etched foil, which allows some parts of it, namely the beams, to extend to the bearing sleeve and to generate a compliant foil. Such a foil is represented in Figure 2.3. Once the journal starts rotating, this foil can slide across the bearing case. This action generates most of the bearing's damping [12].

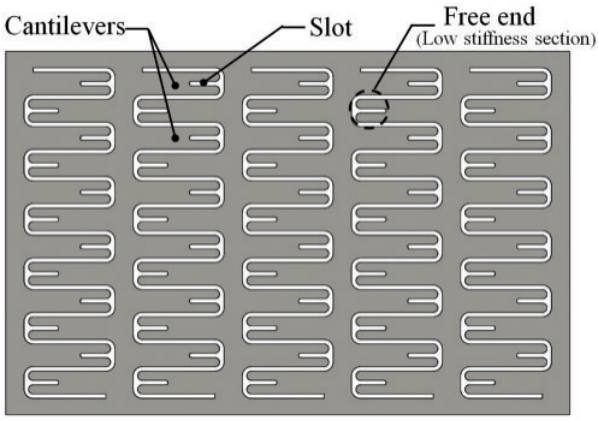

Figure 2.3: Cantilever foil from the Feng et al. study [17].

Feng et al. [17] performed a series of static and dynamic load tests to compute the stiffness and equivalent viscous damping of such a bearing, illustrated in Figure 2.4. The static tests showed that the static stiffness behaves non-linearly and that the bearing has good energy dissipation capacities. This allows to reduce wear at the start and stop phases of its operation. The non-linear static stiffness also prevents large deflection of the journal. As for the dynamic tests, they demonstrated that the damping and dynamic stiffness heavily depend on the excitation frequency.

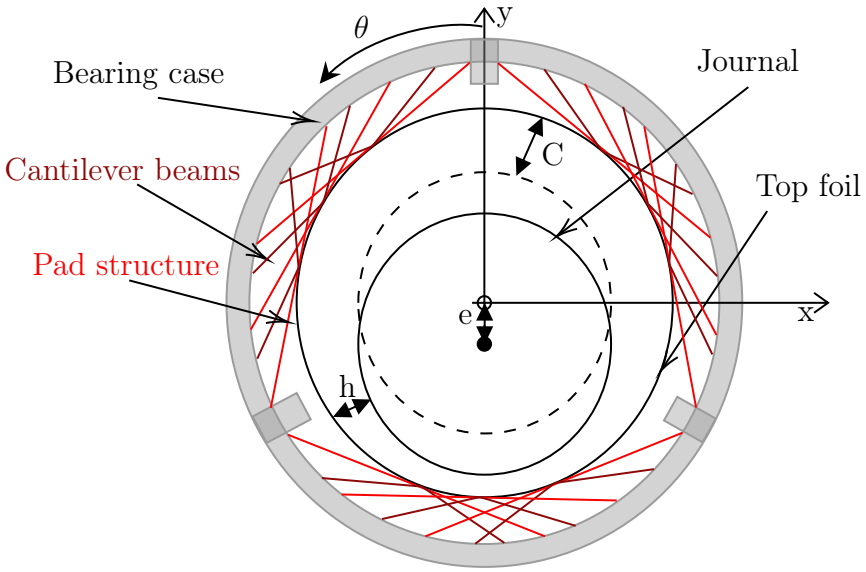

Figure 2.4: Cantilever gas foil bearing.

Obaseki et al. [18] developed a theoretical model to analyse multi-cantilever bearings by using data from the prototype of Feng et al. [17] to validate and carry out their analysis.

2.1.1.3 Advanced Gas Foil Bearing Configurations

As above-mentioned, a lot more different configurations of GFBs exist. Some of them will be briefly presented and shown.

Hybrid Gas Foil Bearing

Hybrid gas foil bearings rely on an external supply of gas to strengthen the gas film in order to increase stability, load capacity, dynamic and static properties of the GFB [19, 20].

Compression Spring Gas Foil Bearing

Compression spring GFBs, represented in Figure 2.5, replace the bump foil by a series of springs clamped into the bearing sleeve, which allows for a parameterisation of the stiffness around the bearing by tuning the different springs [12, 21].

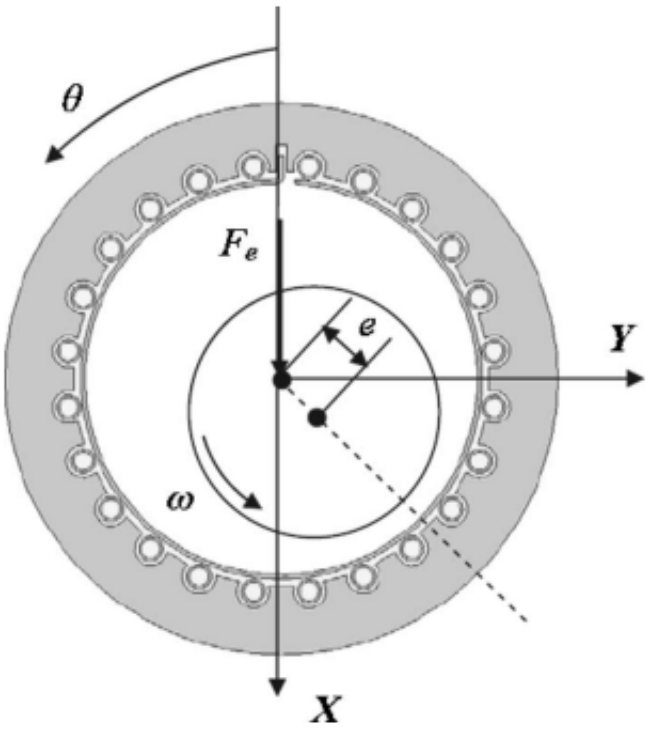

Figure 2.5: Compression springs GFB [21].

Double-arrow Structure Gas Foil Bearing

The very recent and complex novel GFB developed by Feng et al. [22] is made of double-arrow structures filled with damping materials resulting in a negative Poisson's ratio structure to investigate and improve damping and stiffness characteristics of GFBs. This configuration is shown in Figure 2.6. A finite element model of the top foil was used in parallel with the Reynolds equation for the fluid film and a model for the double-arrow structure to develop a numerical model, which was compared to experimental data.

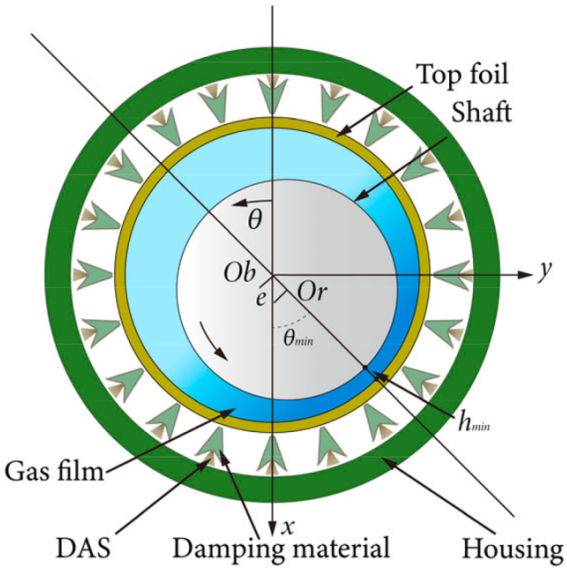

Figure 2.6: Double-arrow structure GFB configuration [22].

Metal Rubber-bump Foil Gas Journal Bearing

The *Metal Rubber-Bump Foil Gas Journal Bearing*, shown in Figure 2.7, was created by Zhang et al. [23]. The particularity of this bearing is that its bump foil is incorporated with periodic "metal rubber damping elements" in between bumps, with the purpose to improve the operational stability and load-carrying capacity of the GFB.

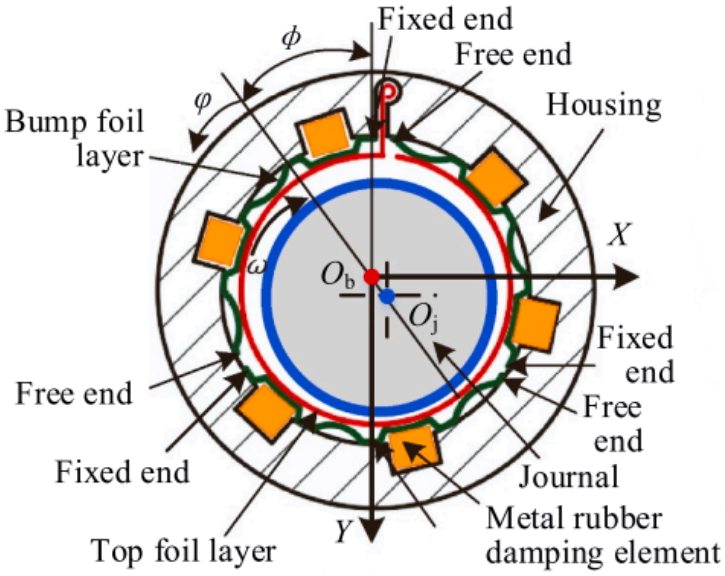

Figure 2.7: Metal Rubber-Bump Foil GFB [23].

2.1.2 Thrust Foil Bearings

Thrust foil bearings present the same advantages and rely on the same working principles as the other bearings already discussed. They are made of several pads named petal equivalent to the top foil for the other bearings. There is a bump foil underneath each petal, as it was the case for the multi-pads bump gas foil bearing. Any compliant or equivalent system could be used. The major change compared to journal GFBs is that the fluid is dragged in the converging channel by the rotation of the thrust runner mounted on the shaft and parallel to the bearing's top foil [24, 25]. Such a bearing is represented in Figure 2.8.

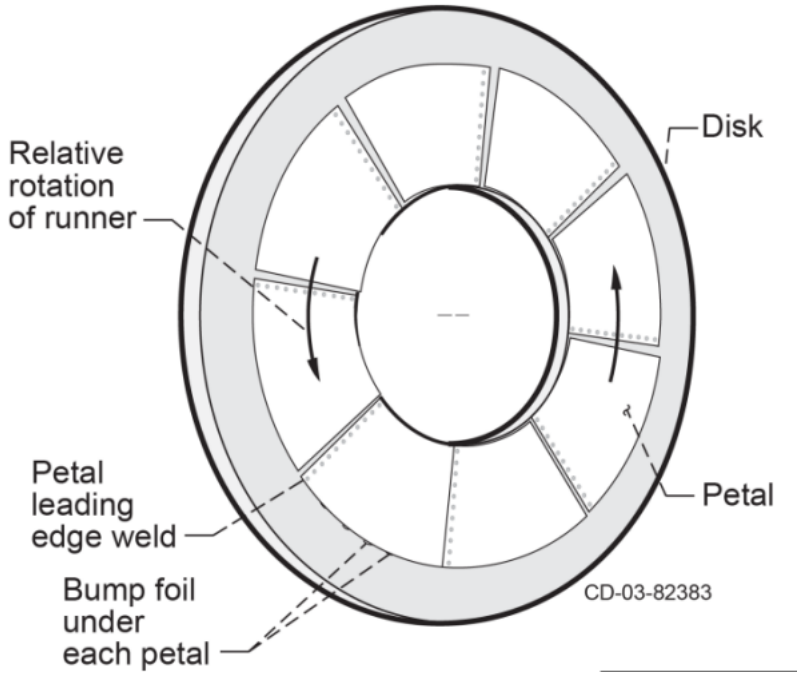

Figure 2.8: Thrust gas foil bearing [24].

2.2 Structural Modelling of the Top and Bump Foils

In his work, Alshikh Saleh Ammar [26] worked on the bump gas foil bearing type and presented three different models to represent the foil structure.

2.2.1 Simple Elastic Foundation Model (SEFM)

All three models and most of the literature about compliant modelling use a form of the simple elastic foundation model (SEFM). The SEFM is based on the hypothesis that the stiffness of the bumps is uniformly distributed on the bearing's surface. Formulations of the SEFM can be differentiated by how the stiffness of the bumps is analytically computed.

2.2.1.1 Wallowit and Anno

The first formulation of the SEFM is the one developed by Wallowit and Anno originally presented in the work of Heshmat et al. [27]. They pose the hypothesis of a single bump of constant stiffness and independent of the number of bump deflections. It is also assumed that the top foil does not sag between bumps and does not have any bending or membrane stiffness, which is equivalent to ignoring it. This model also ignores the friction by setting a zero friction coefficient. The deflection of the foil under the acting forces' effects is only dependent on the local effects, i.e. on the force acting directly over the specific point.

These structural modelling assumptions combined with the additional hypothesis that the gas in the fluid film is isothermal and behaves like a perfect gas, give the following evaluation of the adimensional deflection of the compliant foil $\tilde{h}$:

$$\tilde{h} = \alpha(\tilde{p} - 1), \tag{2.1}$$

$$\alpha = \frac{2p_a s_b}{CE_b} \left(\frac{l_b}{t_b}\right)^3 (1 - \nu_b^2), \tag{2.2}$$

where $\tilde{p}$ is the adimensional pressure applied at the evaluated point, α is the compliance of the foil, which has been adimensionalised with the clearance of the bearing C and the ambient pressure p_a [26, 27]. Other variables with the subscript "b" refer to the bump foil material properties and are respectively: s_b bump pitch, E_b Young's modulus, l_b bump length, t_b bump thickness, ν_b Poisson's ratio.

With this modelling of the compliant foils, the initial solution, i.e. the pressure field at the start of the numerical analysis, must be well defined, as a zero pressure field would lead to a high deflection towards the journal, which is not physically accurate.

However, in the work of Marc Carpino, Lynn A. Medvetz and Jih-Ping Peng [28], which investigated the effects of membrane stresses in GFBs performance, it was concluded that membrane stresses present in the top foil are not trivial in case of highly loaded journals, i.e. with high eccentricities, and that structural models of elastically supported GFBs must consider membrane stresses to predict accurately GFBs' performance.

2.2.1.2 Iordanoff

A few years later, in 1998 [29] and in 1999 [30], I. Iordanoff presented a simplified model in contrast to direct modelling requiring long calculation times. As did Wallowit and Anno, Iordanoff assumed that the top foil does not sag, follows the bump foil in its deformation and does not interact with the bump foil. With this set of assumptions, the deflection is only dependent on the bump foil. As it was shown by Ku and Heshmat [31] [32], the compliance follows a quasi-linear distribution. For his formulation, Iordanoff assumed a linear distribution of the compliance starting with the semi-welded bump with the lowest compliance to the free end bump. The local bump compliance is calculated by taking into account the coulomb friction forces between the bump foil and the bearing support. However, the interactions between bumps are neglected. Iordanoff showed that for constant local compliance S, the entrance film thickness H_1 is the only varying parameter.

Iordanoff's formulations of the compliance for the free end and the semi-welded end of the bump foils are:

$$\alpha_f = \frac{6 p_a s_b I(\theta_b, \mu_f)}{C E_B \sin^3 \theta_b} \left(\frac{l_b}{t_b}\right)^3 (1 - \nu_b^2), \tag{2.3}$$

$$\alpha_w = \frac{12 p_a s_b J(\theta_b, \mu_f)}{C E_B \sin^3 \theta_b} \left(\frac{l_b}{t_b}\right)^3 (1 - \nu_b^2), \tag{2.4}$$

where α_f is the compliance of the free end bump and α_w of the first bump of the pad, which is semi-welded to the bearing casing. $I(\theta_b, \mu_f)$ and $J(\theta_b, \mu_f)$ are two functions depending on the geometry of the bumps and are developed in Appendix A, θ_b is the bump angle and μ_f is the friction coefficient.

However, Xu et al. [33] theoretically derived and experimentally showed the importance of top foil sagging on the pressure field of the gas film and the choice of top foil characteristics. Top foil sagging is noteworthy and cannot be ignored for accurate behaviour predictions. Furthermore, the neglect of any interaction between bumps also induces an error and a reduction in stiffness that could be modelled by globalised models, such as finite element methods or the analytical model developed by Lez et al. [34] and presented in subsection 2.2.2.

2.2.1.3 Larsen and Santos

Finally, the last SEFM structural model is the one from the PhD thesis of Larsen and its supervisor Santos [10]. This model proposed a novel modelling method with a correction term added to the SEFM formulation of Wallowit and Anno to account for the top foil sagging by assuming a periodic bump distribution. However, this hypothesis limits the model to some cases, e.g. models with an inlet slope or multiple pads.

This correction term accounting for top foil sagging is:

$$\alpha_t \approx \frac{p_a s_b^4 (1-\nu^2)}{C E_b t_t^3} \left(\frac{1}{60} - \frac{3}{2\pi^4} \cos \frac{2\pi\tilde{\theta}}{s_b} \right), \tag{2.5}$$

where the subscript "t" refers to the top foil parameters. This correction term of the compliance is then added to the Wallowit and Anno's compliance α from Equation 2.2 to compute the total compliance from the coupling of the top and bump foils.

The three above-mentioned models allow for an efficient and rapid estimation of the stiffness of the bearing, but can lack precision and accuracy, which are required for industrial applications or dynamic analysis. Moreover, the first two of these models completely neglect the top foil and the last model is restricted to only some GFB configurations.

2.2.2 State-of-the-art of GFB's Compliant Modelling

Structural models presented up to this point has always ignored the interactions between bumps, and were all localised model, i.e. models that only consider local effects to compute the deflection of the foils.

Lez et al. [34] developed a globalised structural modelling of the foils by considering the foils as a system of bumps interacting with each other. Each bump is modelled with three degrees of freedom (DOFs) and they are linked to each other with elementary springs. Each bump has one vertical DOF and two horizontal DOFs, which is the minimum required for bumps to be linked to each other. Such modelling is represented in Figure 2.9. The elementary stiffnesses are evaluated and then a global stiffness matrix is computed so that the static equation can be solved by taking friction into account. This model estimates stiffer foils compared to previous analytical models, which were ignoring the interaction between bumps but it still neglects the effect of the top foil.

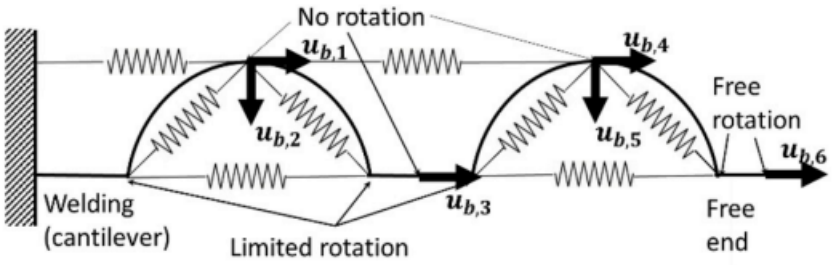

Figure 2.9: Three DOFs bump structure for two neighbouring bumps [34].

The model presented by Lez et al. is based on the contact mechanics between the top foil, the bump foil and the bearing casing. However, Fatu and Arghir [35] demonstrated that even for simple loading situations, contact between the three above-mentioned elements is not always ensured and can become loose, which would result in lower stiffness. Their analysis is based on the introduction of manufacturing errors to evaluate their impact on the stiffness of foil structures. They also noted that different types of manufacturing errors have different impacts, with errors in bump height leading up to 40% of stiffness.

Finally, Arghir and Benchekroun [36] proposed a modification to Lez et al. [34] model by taking into account the elasticity of the top foil and three gaps, namely the gap between the top foil and the journal, the one between the top foil and the bump foil and the one between the bump foil and the bearing sleeve. Lez et al. model is thus extended by adding two supplementary DOFs to each bump to model these gaps. The updated modelling is represented in Figure 2.10. This final model can deal with manufacturing errors and allows for a swift and pretty accurate modelling compared to a full-scale finite element modelling.

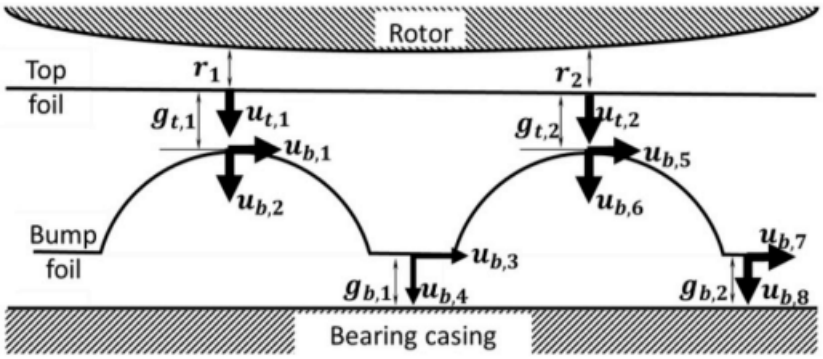

Figure 2.10: Update version with 5 DOFs per bump [36].

More recently, in 2023, Heinemann et al. [19] performed a comparative analysis of four different models for the top foil. In their comparative analysis, the bump foil is every time modelled using a SEFM and the top foil is:

1. neglected, i.e. standard SEFM,
2. modelled as Euler-Bernoulli(E-B) beam elements,
3. modelled as non-curved shell elements,
4. modelled as curved shell elements.

The model employing curved shell elements is used as the benchmark. At steady state journal eccentricities, only low discrepancies between the models are observed. Nevertheless, despite being a simpler model compared to the non-curved shell elements one, the E-B beam element model produces better and thus closer results to the benchmark. This is explained by the fact that the non-curved shell elements model overestimates the axial coordinate dependency. From a stress analysis, it is concluded that this overestimation is due to the neglect of the membrane stresses by this model. This confirms the conclusion already made by Marc Carpino, Lynn A. Medvetz and Jih-Ping Peng [28] on the importance of top foil membrane stresses.

Regarding the time complexity of these four models, the SEFM and the E-B beam elements use about 25% of the time needed by the curved shell elements according to

Heinemann et al.'s analysis. The non-curved shell elements model needs 80% more time than the more complex curved shell elements model. This is most likely caused by the Reynolds equation converging at a slower rate due to large foil deformation, which results from the neglect of the increase of resistance to curvature in one direction caused by the initial curvature of the foil correlated to the membrane stresses.

The compliant foils of novel GFB configurations, such as the ones presented in [22] and [23], also come with their own definitions of stiffness and damping matrices. The structural modelling of such foils cannot be reduced to simple SEFM formulation or other localised solvers. The need for globalised structural solvers is even more important for the analysis and the design of novel high complexity GFBs, which will continue to appear to try and improve GFB's characteristics like load-carrying, stability, damping value, etc.

2.3 Modelling of the Fluid Film

In the context of this work, the fluid film is modelled by using the implementation and mathematical derivation of the steady-state, isothermal Reynolds equation implemented by Alshikh Saleh in the context of his master's thesis in 2021-2022 [26], in the ForDGe solver presented in section 3.1. The Reynolds equation can be solved in 1D or 2D in the incompressible or compressible case for various boundary conditions and is presented in more detail in subsection 3.1.3.

2.4 Conclusion

In conclusion, simpler structural models can be used to gain computation time for preliminary steady-state analysis without losing too much precision, especially for the E-B beam elements which showed promising behaviour.

Nonetheless, for a transient response case, vibration analysis, or in more complex cases, e.g. when using gas injection in the bearing to improve its stability or taking into account the evolution of the top foil from the start-up to liftoff [37], the higher degree of simplification models show some deviations from the curved shell elements model results.

Furthermore, the emergence of various and novel configurations of different GFBs, which can be more and more complex, leads to the development of new structural analysis tools being developed for these new GFBs. The separation of the two solvers, the aerodynamic and the structural ones, offers more flexibility and can allow an easier comparative numerical analysis of different bearing parameters and configurations. Such high-order aerodynamic solvers, like ForDGe, would only require the deformation of the GFB's top foil with respect to the journal as input from the structural solver to compute the pressure field.

Lastly, until now, only localised structural solvers have been linked with ForDGe. Localised models ignore the dependencies between elements, which can lead to inaccuracies, especially for more complex geometries or configurations. Henceforth, coupling with global structural solvers is further needed to perform accurate complex dynamic modelling and this can be more easily achieved if such coupling can be done through a simple Python interface.

Chapter 3

Numerical Modelling

As mentioned in section 1.3, the objective of this thesis is to implement methods and routines in the ForDGe solver to enable its use for GFBs analysis for every kind of bearing or structural modelling for the bearing's foils behaviour. To achieve this, the separation and coupling between the two types of solvers must be well defined.

3.1 ForDGe Solver

3.1.1 General Overview

ForDGe is a discontinuous Galerkin finite element method (DG-FEM) solver developed in the Aerospace and Mechanical Engineering Department of the University of Liège.

This method is a combination of a discontinuous interpolation and a Galerkin variational formulation. The interpolation space is said to be "broken" since its elements consisting of vector functions are fully continuous on each mesh element, but not necessarily across elements. The choice of interpolation basis is thus important and broader than classic continuous finite element method, which imposes that the shape functions are at least once continuously defined across all elements [38].

DG-FEM also presents some advantages over other more common methods such as the finite volume (FV) and the finite difference (FD) ones.

- As above-mentioned, since the continuity across elements is not mandatory, DG-FEM offers more flexibility regarding the choice of shape functions and interpolation orders. This allows for a localised, element-by-element, variable choice of order of interpolation, e.g. the implementation of various subcell methods and blending of different order operators.

- Thanks to its unstructured grid, DG-FEM can manage complex geometries very well.

- DG-FEM satisfies the conservation of conservative variables at the element level, i.e. locally.

All these advantages make the DG-FEM a well-suited choice to handle high-order multi-physics problems and problems involving conservation laws requiring high accuracy and high precision.

3.1.2 Mesh Definition

The following development is heavily based on [38]. DG-FEM employs a broken space with no continuity constraints. Therefore, in such unstructured meshes, no element is perfectly aligned to the set of chosen coordinates. To avoid unnecessary complexity when evaluating the volume and boundary integrals, a mapping from the parametric to the physical coordinates is used. This mapping allows a transformation between the parametric coordinates ξ defined in the reference element to the Cartesian coordinates x in the physical element. This Cartesian mesh is, in most cases, defined by the geometry of the element under study. Such a mapping is shown in Figure 3.1.

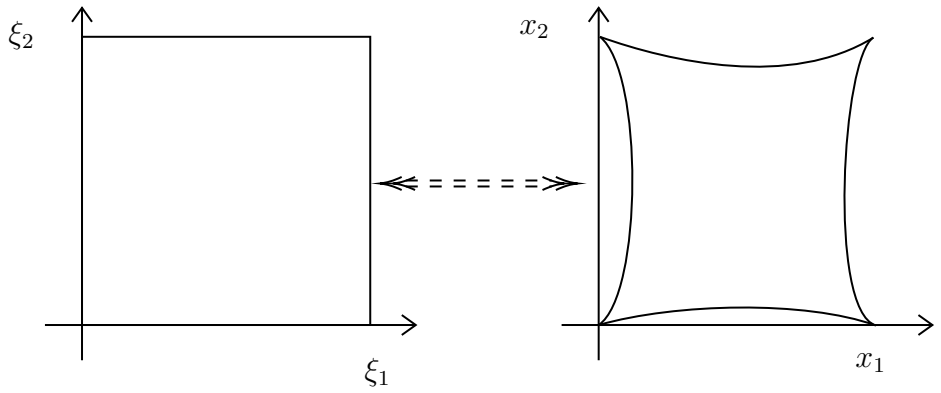

Figure 3.1: Mapping between the reference element and the physical one

To be able to express the solution as a function of the physical coordinates, the solution has to be mapped back to the Cartesian mesh. The existence of the inverse mapping is mandatory and assured by the condition that the mapping Jacobian $\mathcal{J}$ cannot be equal to zero, as the inverse mapping Jacobian $\mathcal{I}$, which defines the inverse mapping, is simply the inverse of $\mathcal{J}$.

$$\mathcal{J}^e_{ij} = \frac{\partial x^i}{\partial \xi^j} \tag{3.1}$$

$$|\mathcal{J}| > 0 \tag{3.2}$$

$$\mathcal{I}^e = (\mathcal{J}^e)^{-1} \tag{3.3}$$

The solution $u(\xi)$ is expressed and computed in terms of parametric coordinates for each element. The physical derivatives of a function f, such as the solution, are obtained from the parametric system by simply applying the chain rule and as for the integration over the element, it only requires $\mathcal{J}$.

$$\frac{f}{\partial x^k} = \frac{\partial f}{\partial \xi^l} = \frac{\partial \xi^l}{\partial x^k} \tag{3.4}$$

$$\int_e f(x)dx = \int_e f(\xi)|\mathcal{J}^e|d\xi \tag{3.5}$$

3.1.3 Gas Film Modelling

The gas film is modelled by the implementation of the Reynolds equation in ForDGe. The following developments are based on Saleh's work in which he applied the DG-FEM to the steady-state, two-dimensional Reynolds equation for an isothermal, isoviscous ideal and compressible gas in ForDGe [26]. In vector form, this equation is written:

$$\nabla \cdot (-\tilde{p}\tilde{h}^3 \nabla \tilde{p}) + \nabla \cdot (\tilde{p}\tilde{h})\mathbf{s} = 0, \tag{3.6}$$

where $\mathbf{s}$ is the advection vector $\mathbf{s} = \{\Lambda, 0\}$ and $\Lambda = \frac{6\mu\omega}{p_a(R/C)^2}$ is the compressibility, with ω the rotation speed, μ the gas' viscosity and R the journal radius. The following summarises Reynolds equation formulation for different cases:

- Incompressible case:

$$\text{1D: } \frac{\partial}{\partial\theta}\left(-\tilde{h}^3\frac{\partial\tilde{p}}{\partial\theta}\right) + \frac{\partial}{\partial\theta}(\Lambda\tilde{h}) = 0, \tag{3.7}$$

$$\text{2D: } \nabla \cdot (-\tilde{h}^3 \nabla \tilde{p}) + \nabla \cdot \tilde{h}\mathbf{s} = 0. \tag{3.8}$$

- Compressible case:

$$\text{1D: } \frac{\partial}{\partial\theta}\left(-\tilde{p}\tilde{h}^3\frac{\partial\tilde{p}}{\partial\theta}\right) + \frac{\partial}{\partial\theta}(\Lambda\tilde{p}\tilde{h}) = 0, \tag{3.9}$$

$$\text{2D: } \nabla \cdot (-\tilde{p}\tilde{h}^3 \nabla \tilde{p}) + \nabla \cdot (\tilde{p}\tilde{h})\mathbf{s} = 0. \tag{3.10}$$

The application of the DG-FEM to this equation requires the computation of the volume and interface fluxes as well as the computation of the source terms. The numerical fluxes are computed using the upwind flux scheme. More detailed explanations and mathematical developments can be found in [26].

As for the boundary conditions (BC), in most cases, Dirichlet's BCs are imposed at the leading and trailing edges of each pad. In this case, the pressure is forced to be equal to the ambient pressure, i.e. $\tilde{p} = 1$. In two-dimensional cases, the pressure is once again fixed equal to the ambient pressure at the edges of the bearing. But the implementation also allows for the use of Neumman and periodic BCs.

3.1.4 Solution Evaluation

In the DG-FEM, as in any finite element method, the space is discretised with a mesh as support. The major particularity of the DG-FEM is that its function space does not need to be continuously defined across elements, but only to a single element. Shape functions ϕ_i, which are the basis of the function space, can therefore be specialised to belonging only to a given element ϕ_i^e.

In FEM, the solution $\mathcal{U}$ is approximated by the finite element space $\mathcal{U}_h$, where h denotes the mesh size:

$$\lim_{h \to 0} \mathcal{U}_h = \mathcal{U}. \tag{3.11}$$

The approximate solution is then computed as the expansion of the shape functions:

$$u_h^e(x) = \sum_{i=1}^{N} u_i^e \phi_i^e(x), \tag{3.12}$$

in ForDGe, the shape function basis chosen is the Lagrange polynomials, their use in DG-FEM is mainly motivated by a reduced operation count during computation since the continuity does not need to be enforced [38].

Consequently, the shape functions are:

$$\phi_k(x) = L_k(x) = \prod_{\substack{i=0 \\ i \neq k}}^{N} \frac{x - x_i}{x_k - x_i}, \tag{3.13}$$

where x_i are the interpolation points and $k \in [0, 1, \ldots, n]$. In ForDGe, Lagrange interpolants can either be based upon equidistant points or upon the Gauss-Lobatto-Lengendre (GLL) control points, the GLL control points are represented in Figure 3.2, as they are chosen over the equidistant ones in the frame of this work since they provide an optimal set of interpolation points for high order of interpolation [26].

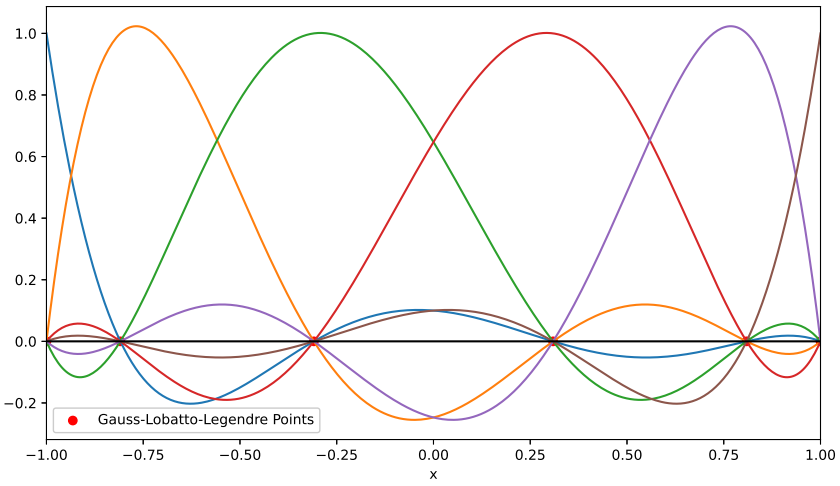

Figure 3.2: 6th order Lagrange polynomials and their associated GLL control points.

3.2 Coupling of Solvers

In such multi-physics problems, one of the most important points is the way how both solvers are coupled. Given that the structural solver could be led to change a lot depending on the GFB or the choice of modelling of the bump or top foils, the coupling should remain flexible, while still being straightforward. Consequently, the choice to use the adimensional gap $\tilde{h} = \frac{h}{C}$ as the communicating parameter is made. This gap is fed to ForDGe to compute the adimensional pressure field $\tilde{p} = \frac{p}{p_a}$. Subsequently, the pressure

field would be given to the structural model, which would compute the deflections of the bearing's foils due to the pressure field and so on.

This type of coupling is naturally an iterative process. Before the startup, the bearing is tightened on the journal, the gas pressure is non-existent inside the bearing and the gap is equal to zero. Numerically, it would be very complex to dynamically compute the liftoff transition of a GFB. Thus, a way to avoid such a problem is to assume an initial non-zero gas film pressure field, with the idea that the static equilibrium operation point would be reached iteratively, whatever the initial conditions are.

Indeed, the action of the pressure on the foils and their deformation in response to it acts as a feedback loop. If the pressure is too high, the gas film will push back on the top foil deflecting it and thus reducing the pressure. The opposite also stands true, as a low pressure would allow the compliant foil to deflect back and reduce the gas film volume, consequently increasing the pressure. One can intuitively guess that there exists a stable equilibrium between the foil deflection and the pressure field.

3.3 Structural Solver Externalisation

Some simple structural solvers were already implemented in ForDGe, as discussed and presented in chapter 2. However, it would be difficult to implement and adapt the inner workings of ForDGe to each structural model that could be used. This is another reason why structural solvers need to be extracted out of ForDGe.

This externalisation requires data communication between the solvers and a process handling this transfer of information. The communication has been designed to be handled by a Python interface. ForDGe's pressure field is passed to this interface, which receives the data and sends it back to any structural solver. The structural solver can compute the deflections of the bump foil and/or top foil from the pressure field it got. It then sends

them back to the Python interface for the next iteration so that ForDGe can update the pressure field.

However, both solvers could, and most likely would, use different meshes, mesh types or even different orders of interpolation. It is important to avoid losing accuracy during the manipulation of the data and their modification from the source mesh to the target one. To ensure that the data stay relevant despite these modifications, the Python interface gives ForDGe the data point of the field at which the pressure will be needed by the structural solver, such that ForDGe can compute the exact pressure values at these points instead of an approximation. This computation is made by using directly ForDGe's shape functions and computing the pressure field by transforming the external coordinates to the local, element-wise, coordinates. Once the solution, i.e. the pressure field, has been evaluated in the parametric coordinate system, it can be computed back on the physical one as described in subsection 3.1.2.

As for the gap $\tilde{h}$, it is computed by the structural solver on its own mesh, i.e. the above-mentioned data points or external coordinates, and passed as such to ForDGe. Hence, interpolation is required between both meshes to allow the gap to be read by the aerodynamic solver. This process is done by a bilinear interpolation. This choice of interpolation is made to benefit from the advantages of such a method. The bilinear interpolation is time efficient for a reasonable accuracy, which is useful as the gap interpolation will be required each time the Reynolds equation is solved.

3.4 Structural Solvers

3.4.1 General Requirements

The only requirement for any structural solver to be linked with ForDGe is to be able to:

- communicate with a Python interface,
- provide it with its mesh information,
- receive the pressure field as an input from this interface,
- and send it the resulting deformation of the compliant foil(s).

As the objective is to externalise the structural solvers from ForDGe, the three simpler models, i.e. the SEFM formulations of Wallowit and Anno, the one of Iordanoff and the one of Larsen and Santos, all three have been implemented in Python to verify the validity of the methodology and to assess its accuracy. Furthermore, a simple beam finite element model (FEM) has been implemented in Python as well to compute and evaluate the impact of the top foil modelling, which had been ignored until now with the exception of Larsen and Santos' model, even though the latter also had its limitations. These results and validation will be presented and discussed in chapter 4.

3.4.2 Beam Element Modelling

In the context of this work, a beam FEM model has been implemented to further validate the externalisation process of the structural solvers. This implementation is based on the mathematical derivations found in [19, 39]. The top foil is discretised in a series of N_e elements of length l_e. The pressure acting on each of the elements is received from the coupling interface to express it as the load vector. Nevertheless, as only a static analysis is performed, only the globalised stiffness matrix construction procedure is required, since the equation of motion of a beam in static analysis is reduced to:

$$\mathbf{Kx} = \mathbf{f}, \tag{3.14}$$

which is a simple linear system including the globalised stiffness matrix $\mathbf{K}$, the degrees of freedom (DOFs) $\mathbf{x}$ load vector $\mathbf{f}$. The globalised stiffness matrix can be built directly by summing each elemental stiffness matrix $\mathbf{K^e}$:

$$\mathbf{K^e} = \frac{E_t I_t}{l_e^3} \begin{bmatrix} 12 & 6l_e & -12 & 6l_e \\ 6l_e & 4l_e^2 & -6l_e & 2l_e^2 \\ -12 & -6l_e & 12 & -6l_e \\ 6l_e & 2l_e^2 & -6l_e & 4l_e^2 \end{bmatrix}, \tag{3.15}$$

$$\mathbf{K} = \sum_{e}^{N_e} \mathbf{K^e}, \tag{3.16}$$

where I_t is the bending inertia of the top foil.

Each node between the elements is attributed two DOFs, the vertical displacement of the node as well as its rotation. Once the globalised matrix $\mathbf{K}$ is computed, various boundary conditions can be applied to the beam by constraining some specific DOFs. The two cases discussed in section 4.2 are the cantilever beam and the periodic BCs. For two-dimensional analysis, this model averages the pressure in the axial direction. The model could be extended to a plate FEM to avoid this reduction.

3.5 Iterative Process

In this section, the iterative process of the coupling will be discussed and explained in more detail. The algorithm is represented in Figure 3.3.

The first step is to estimate an initial solution of the pressure field $\tilde{p}_{\mathrm{F}}$ to avoid the transition period between the startup and the liftoff. The simplest choice is to assume a constant pressure field of ambient pressure, which is a reasonable assumption as the pressure outside the bearing is the atmospheric pressure and the pressure inside the bearing should not exceed nor fall behind this value by much.

This pressure field $\tilde{p}_{\mathrm{F}}$ is interpolated on the structural solver's mesh by the process described in section 3.3. This interpolated pressure $\tilde{p}_{struct}$ is sent to the structural solver, which can now compute the deflection of the foils $\tilde{h}_{struct}$ that is sent back to ForDGe.

One of the main aspects of this externalisation of the structural solvers from ForDGe is the transfer of data between ForDGe and the coupling interface. Whether it is for the transfer of the pressure field from ForDGe to the coupling interface or of the gap after its computation by the structural solver, this data communication is handled by the software *Simplified Wrapper and Interface Generator* SWIG. ForDGe is implemented in C++, while the coupling interface is in Python to facilitate the accessibility of the interface. In the frame of this work, structural solvers are also implemented in Python.

The data must be shared while maintaining as much accuracy as possible, yet the solvers work with different data formats each defined by their own implementation architectures. SWIG allows defining a pairing mechanism for each data type from different programming languages to match different variables from the interface and the solvers. It also enables the definition and use of Python routines from the interface to be called by ForDGe. A more detailed presentation of this mechanism and its implementation is shown in Appendix B.

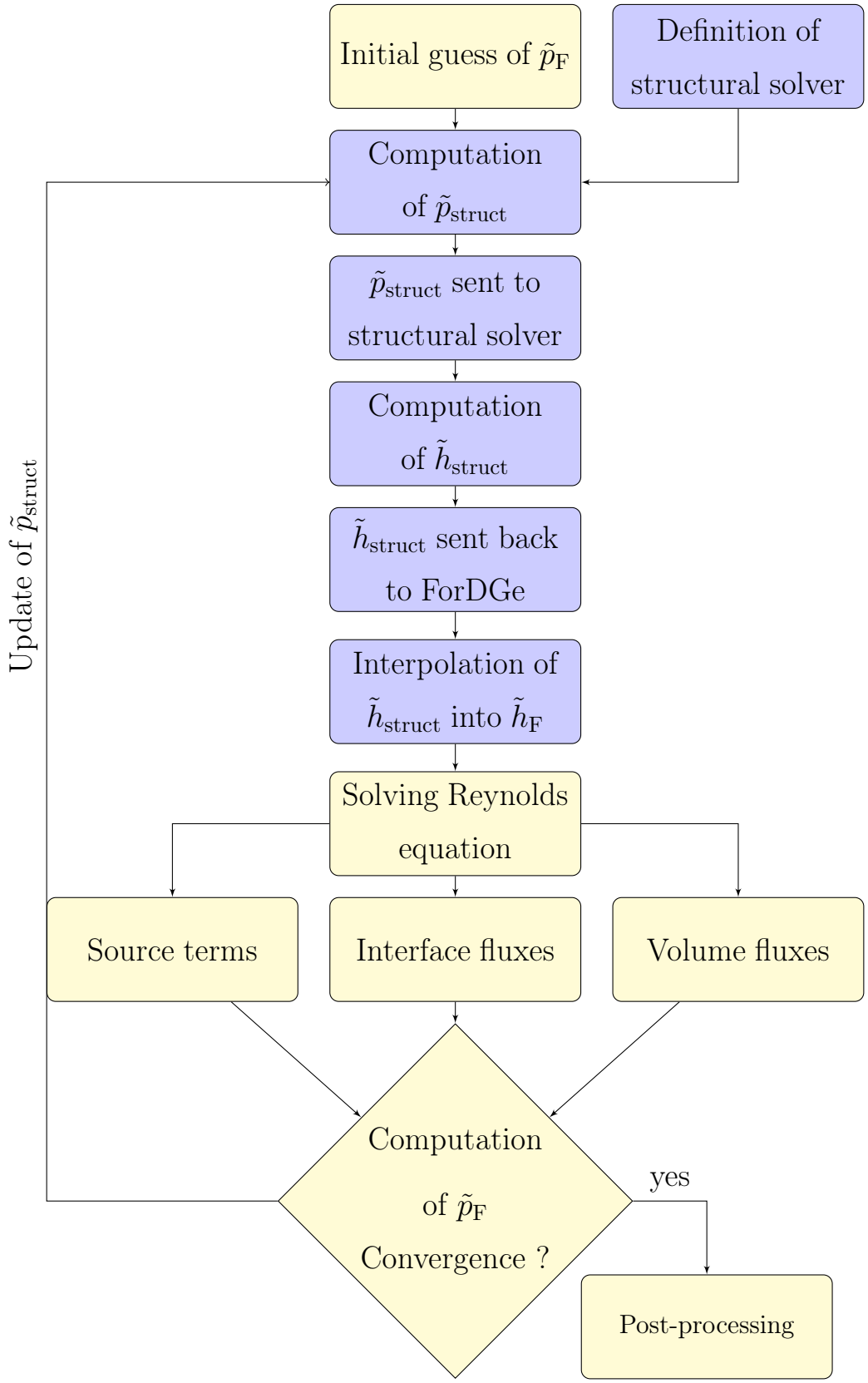

Figure 3.3: Flowchart of the iterative coupling of solvers. The indice "struct" refers to the mesh of the external solver and "F" to the mesh of ForDGe. Blue blocks represent the new steps implemented in the frame of this work.

The $\tilde{h}_{struct}$ is then bilinearly interpolated back to ForDGe's mesh. This field $\tilde{h}_F$ can be used to solve the Reynolds equation. The equation is solved by using a classical Newton-Raphson approach and evaluating the residual, which can be computed in three steps. First of all, the variable(s) and their parametric gradients must be interpreted from the interpolation points to the quadrature ones. Secondly, source terms, volume and interface fluxes must be computed at the quadrature points. Finally, a return from the interpolation points from the quadrature ones is performed. More detail about this procedure and the mathematical derivations are presented in [26, 38, 40].

Finally, the convergence is considered reached once the relative error of the solution between two iterations is smaller than a tolerance factor, i.e. when the following criterion is validated:

$$\left| \frac{p_{j-1} - p_j}{p_j} \right| \leq \text{tol.} \tag{3.17}$$

As for $\tilde{p}_{\text{struct}}$, it is updated each time the residual is computed to avoid having to compute it each time the $\tilde{h}_{\text{F}}$ is required, i.e. at each flux or source term computation.

Chapter 4

Computation Analysis and Validation

4.1 Validation of the Externalisation

The validation of the externalisation methods is performed by comparing results obtained with the structural solvers intrinsic to ForDGe with the same one externalised and implemented in Python, namely Wallowit and Anno, Iordanoff and Larsen and Santos models. The results will be shown for a bump type GFB with a single 360° pad.

4.1.1 Comparative Analysis

In this subsection, the externalised models will be compared to their mirror selves present within ForDGe.

The first model to be compared is Wallowit and Anno's one. The test case is a one dimension mesh with 50 elements for the structural solver and 30 for ForDGe's mesh. The Reynolds equation is solved in the compressible scenario and Dirichlet's boundary conditions have been applied at both ends of the pad. For each solver, external and intrinsic, the pressure field is computed for four different journal eccentricity ratios $\varepsilon = e/C$. The pressure field is represented in Figure 4.1. The dashed and black lines refer to the externalised solver and the continuous lines to the intrinsic solver.

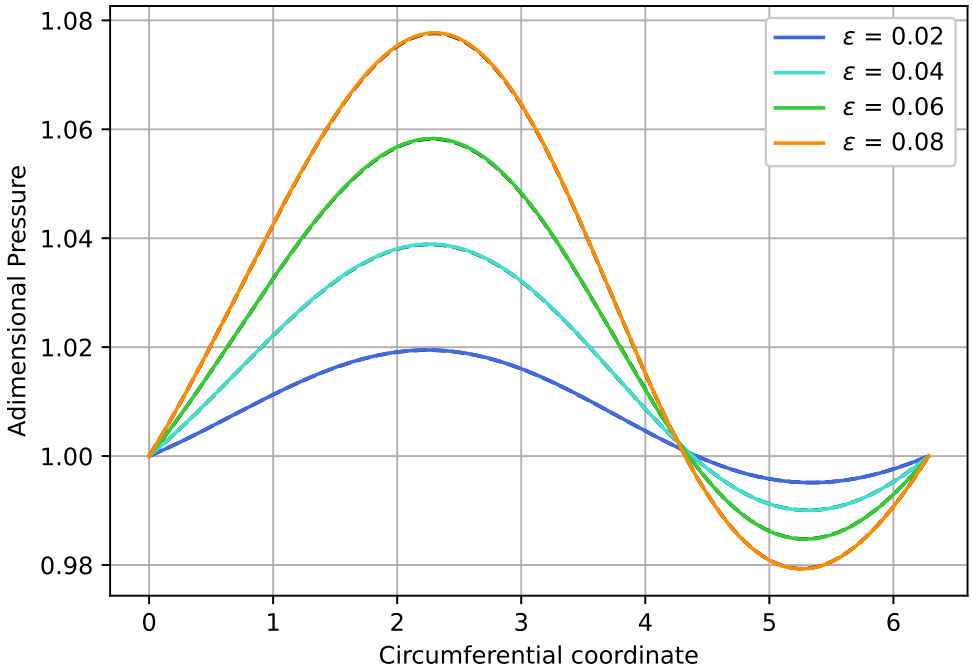

Figure 4.1: Steady-state pressure field at 300°K and 120,000 RPM.

The difference between the intrinsic and externalised structural solvers is highlighted in Figure 4.2. As it can be seen, the externalised Wallowit and Anno's model follows pretty well its counterpart present in ForDGe. The difference between the two models has been computed and is graphically represented in Figure 4.3.

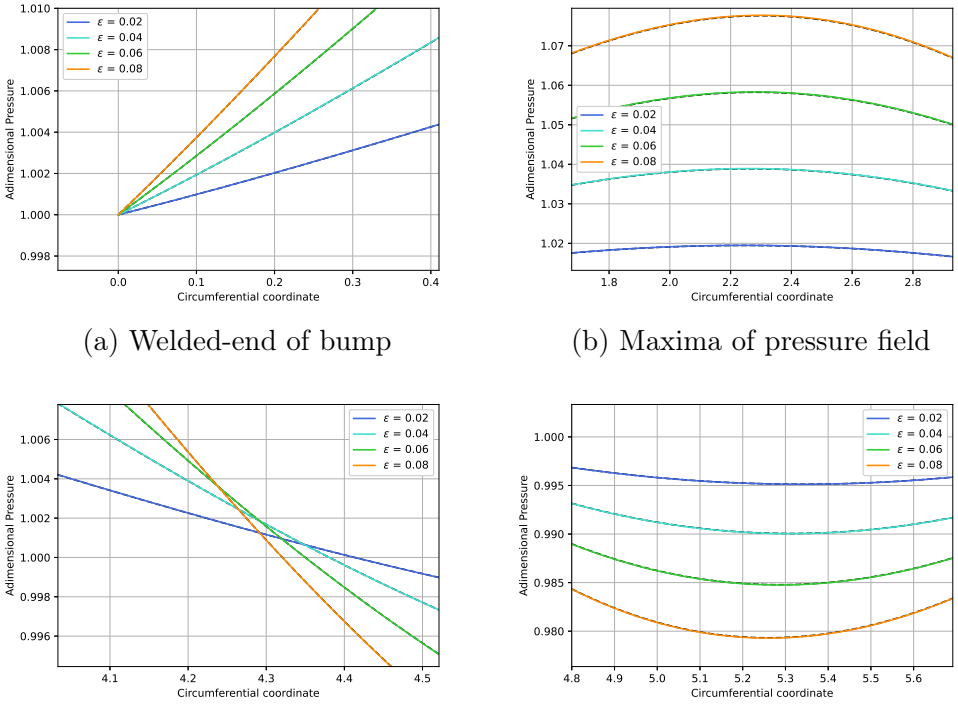

(a) Welded-end of bump

(b) Maxima of pressure field

(c) Inflection point of pressure field

(d) Minima of pressure field

Figure 4.2: Highlighted differences of Figure 4.1, where the dashed black lines represent the externalised solver's solutions.

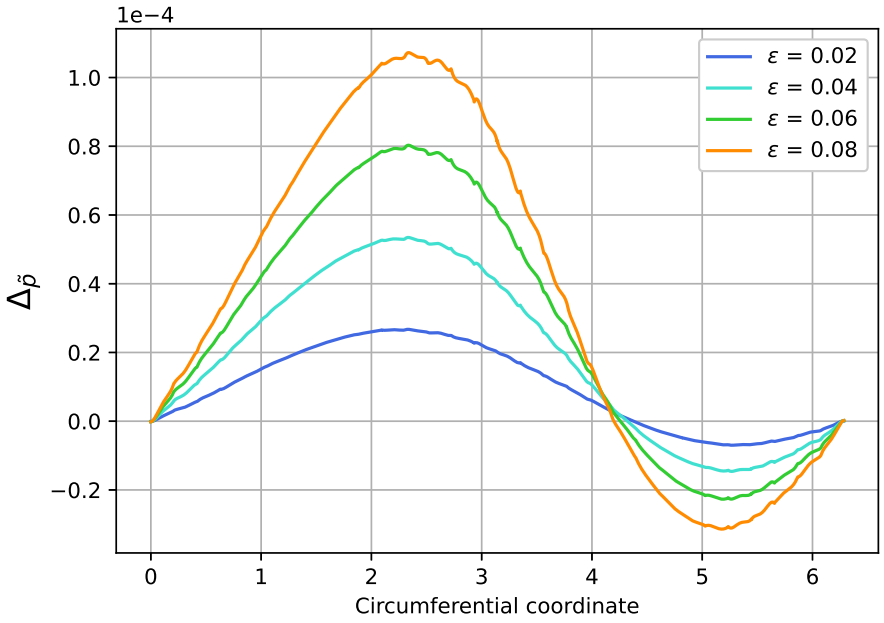

Figure 4.3: Difference between external and intrinsic solvers' pressure fields, where $\Delta\tilde{p} = \tilde{p} - \tilde{p}_{\text{ext}}$, with $\tilde{p}$ referring to the pressure field of the internal structural solver and the subscript "ext" denotes the solution with the external solver.

The biggest difference between the models occurs for the highest eccentricity ratio. This is most likely due to the linear interpolation of the pressure field. Indeed, the higher the eccentricity ratio is, the higher the pressure field maximum and the steeper the slope of the field will be. Thus, in these conditions, the interpolation will introduce the biggest errors near the maxima, as the linear assumption between neighbouring points of such interpolation is not exactly accurate. To measure the difference between the different solvers, the relative errors at the maxima will be computed. The relative error at the maximum pressure is only of $\left|\frac{\tilde{p}_{\text{ext max}} - \tilde{p}_{\max}}{\tilde{p}_{\max}}\right| = 9.952\text{e}^{-5}$ and of $\left|\frac{\tilde{p}_{\text{ext min}} - \tilde{p}_{\min}}{\tilde{p}_{\min}}\right| = 3.206\text{e}^{-5}$ at the minimum pressure.

The same results are expected and seen for the adimensional gap $\tilde{h}$, represented in Figure 4.4 and Figure 4.5, where the dashed lines are barely visible at the minimum gap. The biggest relative error at the minimum gap is $\left|\frac{\tilde{h}_{\text{ext min}} - \tilde{h}_{\min}}{\tilde{h}_{\min}}\right| = 1.782\text{e}^{-4}$.

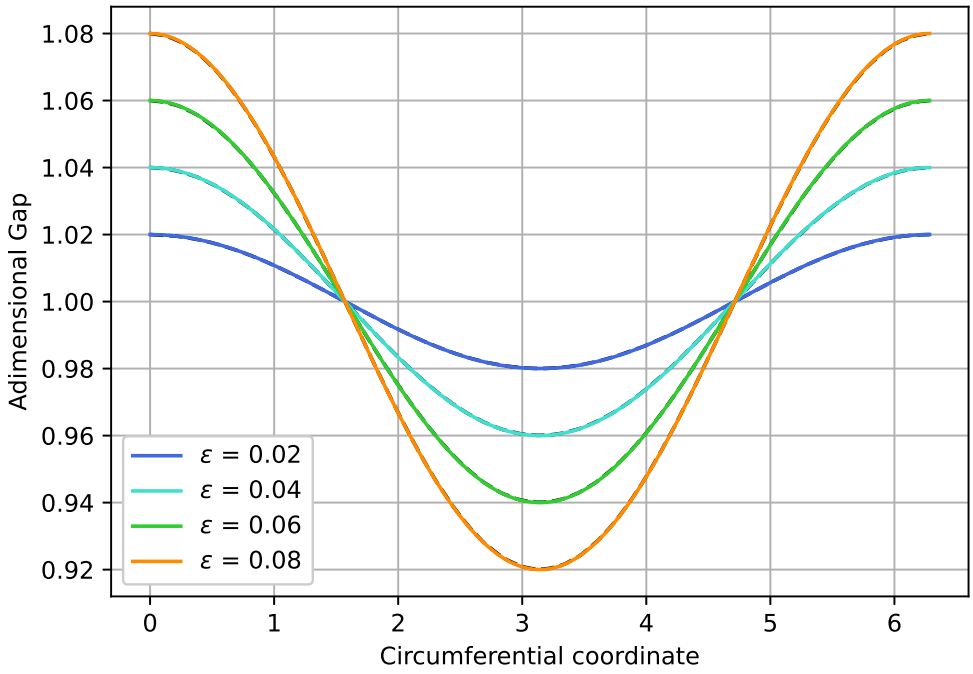

Figure 4.4: Steady-state gap field at 300°K and 120,000 RPM.

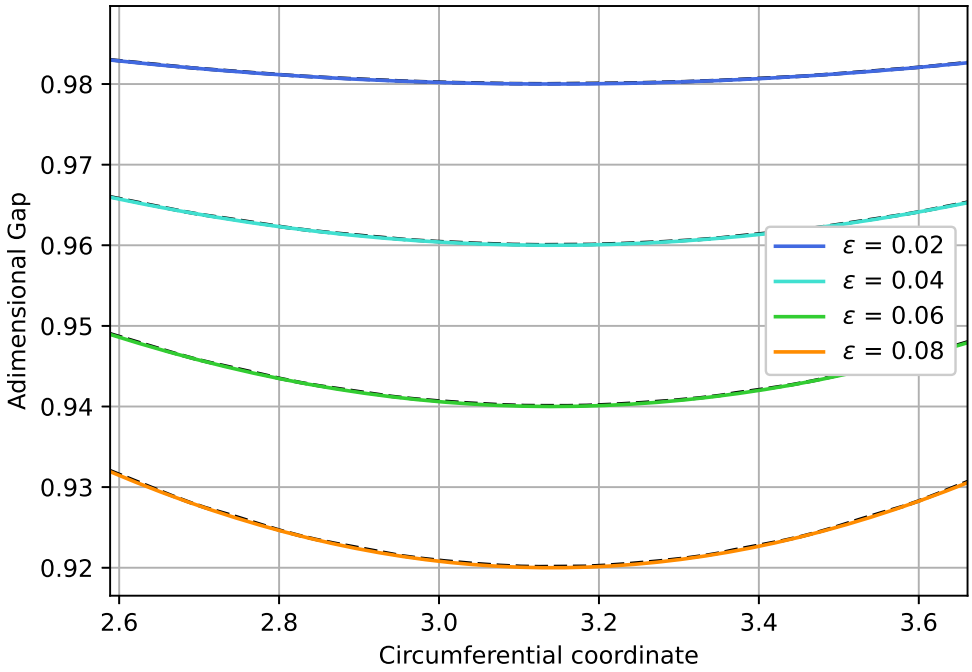

Figure 4.5: Minimum gap for the highest eccentricity ratio of Figure 4.4.

As small as they are, these differences confirm that both models are equivalent, even though one of them is across a Python interface data transfer and a double interpolation, one following the mathematical process presented in subsection 3.1.4 and one linear interpolation, for the 1D case.

Similar behaviour is observed for Iordanoff's model implementation. This result could be expected, as Iordanoff's formulation is simply another way to compute the compliance of a SEFM. The pressure field for the same eccentricity ratios as Wallowit and Anno's model is shown in Figure 4.6, with the maximum discrepancy between the internalised and externalised version being $\left|\frac{\tilde{p}_{\text{ext max}}-\tilde{p}_{\text{max}}}{\tilde{p}_{\text{max}}}\right| = 9.952\text{e}^{-5}$ and $\left|\frac{\tilde{p}_{\text{ext min}}-\tilde{p}_{\text{min}}}{\tilde{p}_{\text{min}}}\right| = 3.206\text{e}^{-5}$.

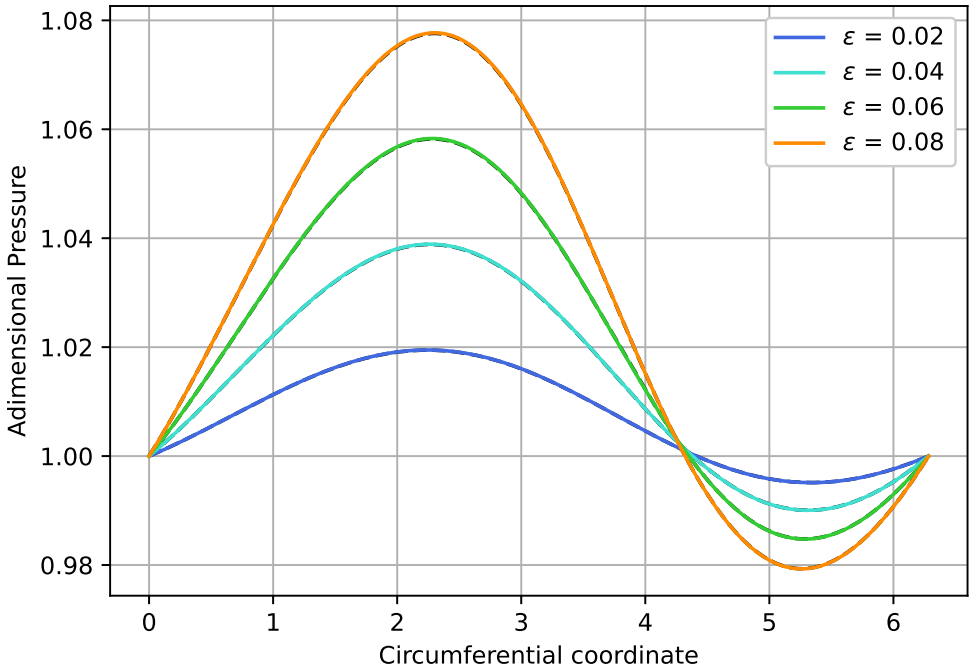

Figure 4.6: Steady-state pressure field at 300°K and 120,000 RPM for Iordanoff's structural solvers.

The same observation can be made for the gap field, but will not be shown here to avoid too much redundancy. However, it is good to note that the biggest discrepancy between models leads to $\left|\frac{\tilde{h}_{\text{ext min}}-\tilde{h}_{\text{min}}}{\tilde{h}_{\text{min}}}\right| = 1.782\text{e}^{-4}$.

It comes out of the comparative analysis of the two above-mentioned solvers that, for a simple SEFM, no matter its absolute accuracy, the error introduced by the externalisation of a SEFM solver for a specific test case can be found by computing the error between the two versions of a same solver. Moreover, it can be highlighted that these errors remain very close for pretty similar solvers such as the Wallowit and Anno's and Iordanoff's models. The errors are equal up to the e^{-10} order, which is the order of precision of the pressure field convergence of the numerical aerodynamic solver, i.e. $tol = \text{e}^{-10}$ from section 3.5. The error introduced by the externalisation can be quite well estimated for SEFM models.

As for Larsen and Santos' model, the correction term used to model the top foil has a too small effect on the steady-state analysis, which leads this model to be very similar to Wallowit and Anno's in terms of error due to its externalisation.

The bearing's and the test case's parameters that were used for this comparative analysis are displayed in Table 4.1.

Parameter	**Value**	**Unit**
Rotation speed	$120 \cdot 10^3$	RPM
Temperature	300	°K
Journal radius	12	mm
Clearance	50	µm
Bump foil length	852	mm
Bump foil pitch	2.17	mm
Bump foil thickness	101.6	mm
Bump angle	1.5386	rad
Bump foil Young's modulus	185	GPa
Bump foil Poisson's ratio	0.29	[-]
Bump foil friction coefficient	0.05	[-]
Top foil thickness	101.6	mm
Top foil Young's modulus	196	GPa
Top foil Poisson's ratio	0.3	[-]

Table 4.1: Bearing's parameters for the test case.

4.1.2 Two-dimensional Case

The structural solver's externalisation has been implemented to support two-dimensional analysis. Validation of two-dimensional models will be presented in the following. The test case for this particular analysis has the same bearing parameters as the one displayed in Table 4.1. The radial direction is modelled as it was in the previous subsection, i.e. in 30 elements for ForDGe's mesh and 50 elements for the externalised structural solver's

mesh. The axial direction is modelled by using 20 elements and 30 for ForDGe and for the external solver respectively. The boundary conditions of the test case force the pressure field to be equal to the ambient pressure p_a at the extremities of the bearing and at the ends of the foils, as it was for the 1D test case. The pressure field is represented in Figure 4.7 and Figure 4.8. In the second one, the solution from the external solver has thicker lines to show good matching, otherwise only one of the colours is seen.

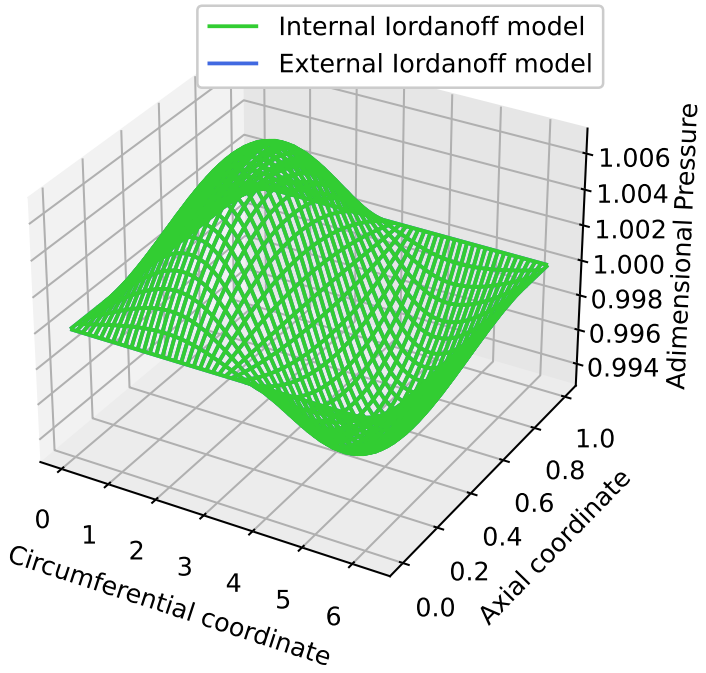

Figure 4.7: Two-dimensional pressure field for $\varepsilon = 0.08$.

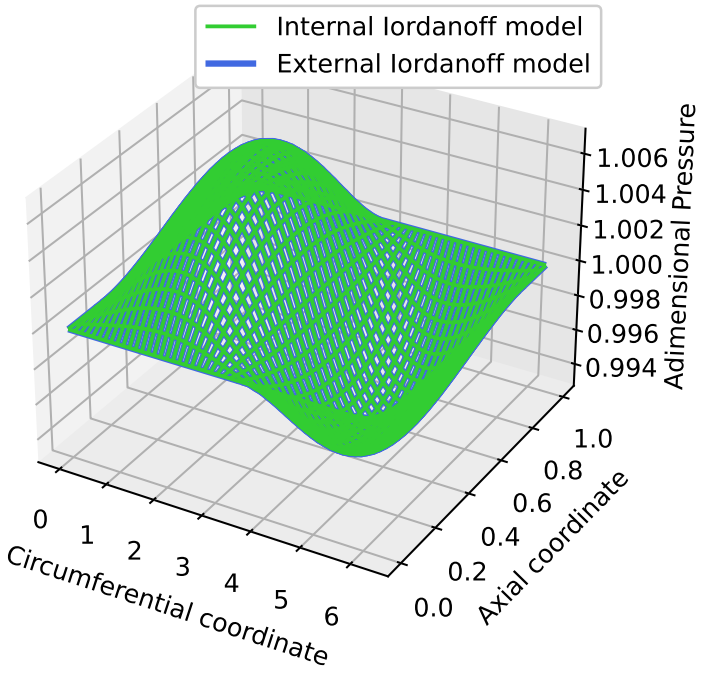

Figure 4.8: Thickened pressure field of Figure 4.7.

Iordanoff's model has been used for both of these representations. The biggest discrepancy between the models occurs at the maximum and minimum values of the pressure field, as it was the case for the 1D analysis. Thus, the differences between the maximum and minimum values of the pressure field have been computed to evaluate the relative error introduced by the externalisation of the structural solver for two-dimensional cases. The relative error at the minimum of the pressure field is $\left|\frac{\tilde{p}_{\text{ext min}}-\tilde{p}_{\text{min}}}{\tilde{p}_{\text{min}}}\right| = 9.98\text{e}^{-6}$ and for the maximum $\left|\frac{\tilde{p}_{\text{ext max}}-\tilde{p}_{\text{max}}}{\tilde{p}_{\text{max}}}\right| = 1.007\text{e}^{-5}$. The corresponding gap field is shown in Figure 4.9.

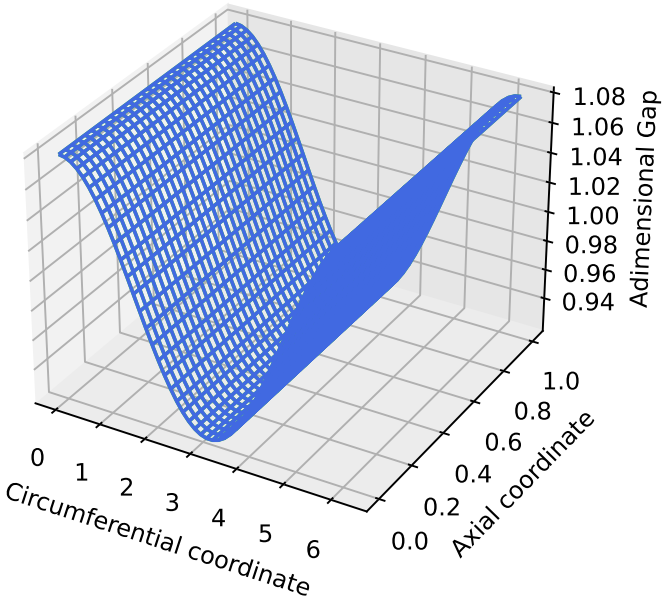

Figure 4.9: Two-dimensional gap field for $\varepsilon = 0.08$

It can be noted that the displacement (Figure 4.9) is constant along the axial direction of the bearing but that the pressure field (Figure 4.7) varies both in the radial and in the axial directions. This is due to the boundary conditions of the test case, which impose the pressure field, i.e. the solution, to be equal to the ambient pressure p_a on the extremities of the bearing as well as the welded and free ends of the foils. The other reason explaining this numerical result is that, as of now, every structural model that has been coupled with ForDGe averages the pressure in the axial direction, which is another reason motivating this externalisation interface for coupling with higher accuracy structural models.

The same conclusion as the one-dimensional test case can be drawn. The relative errors are of the same order and don't seem to be influenced much by the extension to a second dimension of the multi-physics problem. The biggest difference between external and internal models occurs at the maxima, as it was for the one-dimensional analysis. This is most likely due to the bilinear interpolation of the pressure field.

4.1.3 Other Test Cases

The validity of the externalisation has also been insured for different cases, such as the incompressible case, the no foil case, other rotation speeds and different temperature values. Relative errors between external and internal solvers remain somewhat constant, with the exception of increasing pressure amplitude. If the parameters of the test run lead to higher/lower maximum/minimum pressure values, the overshoot/undershoot of the interpolation will cause increasing relative errors for the same reasons mentioned in the above subsections. For instance, when evaluating GFB behaviour under high eccentricity ratios it would be good practice to take the interpolation-induced error into account.

4.1.4 Structured Mesh Convergence Analysis

This analysis has been made to evaluate the effect of the refinement of the structural solver's mesh on the pressure field computation. The convergence analysis is based on Sommerfeld analytical expression for an incompressible case, for a periodic 360° journal bearing with infinite journal length. These assumptions lead to a skew-symmetric pressure distribution [41].

This study is based on the squared relative error of the numerical solution compared to the analytical one computed at each circumferential coordinate and for different numbers of elements N_e for the structured mesh. The parameters of the numerical solution are the ones listed in Table 4.1 and the eccentricity ratio is $\varepsilon = 0.08$. The test case is the 1D incompressible solution with one 360° pad and with 30 elements for ForDGe's mesh. The results of this analysis are shown in Figure 4.10.

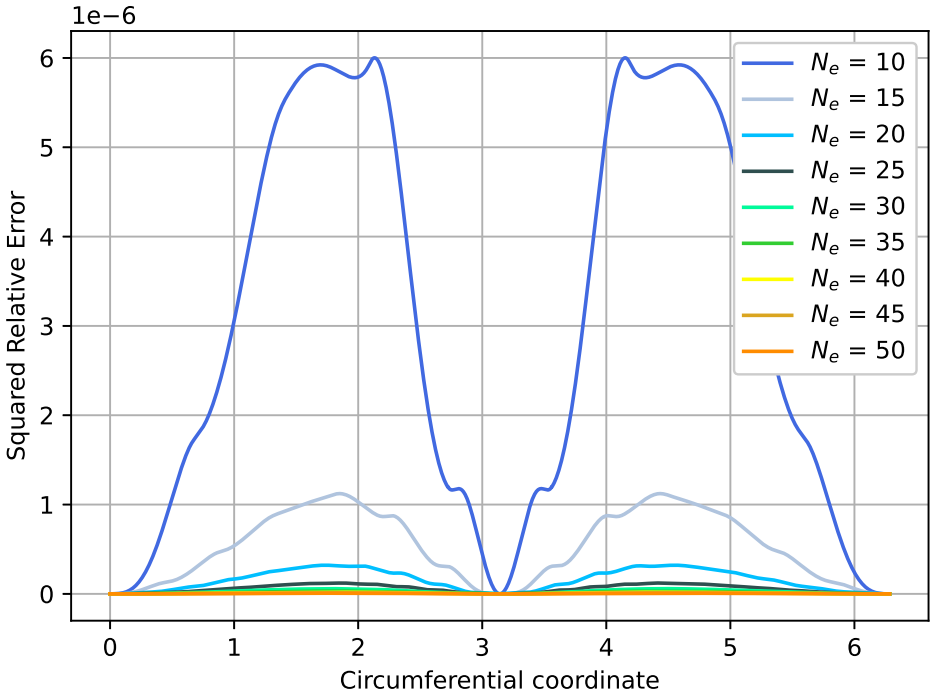

Figure 4.10: Squared relative error of numerical solution compared to Sommerfeld's analytical solution.

It comes out of these results that the number of elements of the structural solver's mesh does have an impact on the accuracy of the solution. However, as soon as N_e tends to or even exceeds the number of elements of ForDGe's mesh, this relative error tends to zero. Consequently, it would be good practice to use a structural mesh at least as refined as ForDGe's input IJK mesh to reduce the coupling induced error as much as possible.

4.2 Effect of Top Foil Modelling

Two models including top foil modelling have been coupled with ForDGe. The first one is Larsen and Santos' model, which is just the addition of a correction term to Wallowit and Anno's SEFM compliance formulation. This term is based on the assumption of a periodic top foil, which can be somewhat limiting in its accuracy to model higher complexity GFB configurations. The other model implemented is the modelling of the top foil by a beam finite element method (FEM). This model has only been implemented

externally to ForDGe.

In the following, both methods will be compared to each other and to a benchmark, which is simply Wallowit and Anno's model. The comparative analysis is based on a test case with the same parameters as the previous sections found in Table 4.1. Furthermore, for every solver, the computations have been performed with the external version of the solvers to put them on equal ground. Also, only one eccentricity ratio $\varepsilon = 0.08$ will be used for clarity. The gap $\tilde{h}$ and the pressure field $\tilde{p}$ are respectively shown in Figure 4.11 and Figure 4.12.

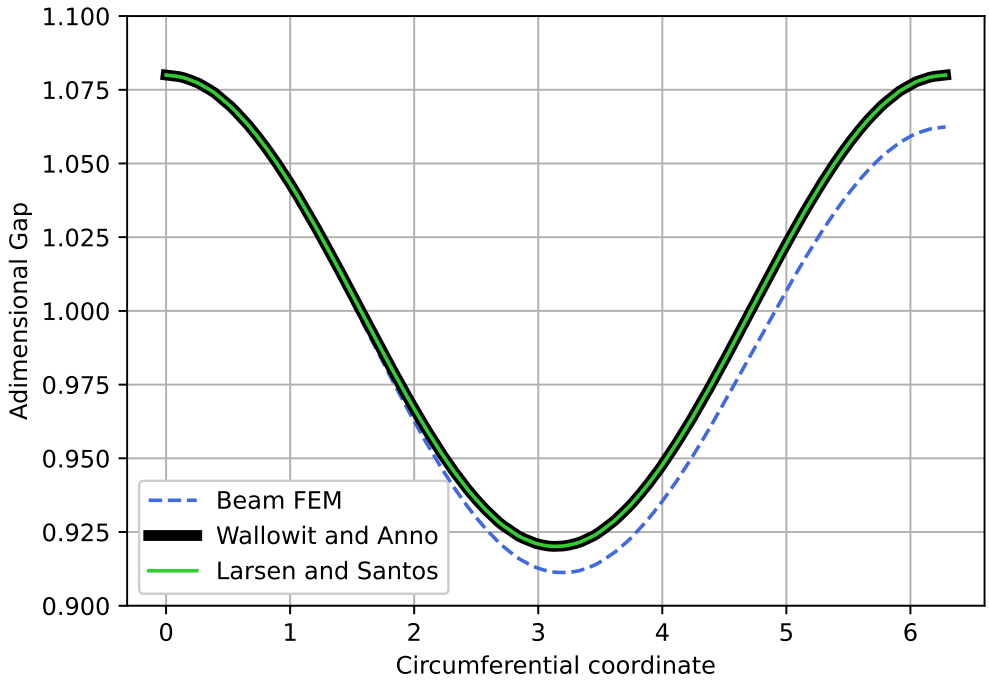

Figure 4.11: Gap field $\tilde{h}$ with top foil modelling.

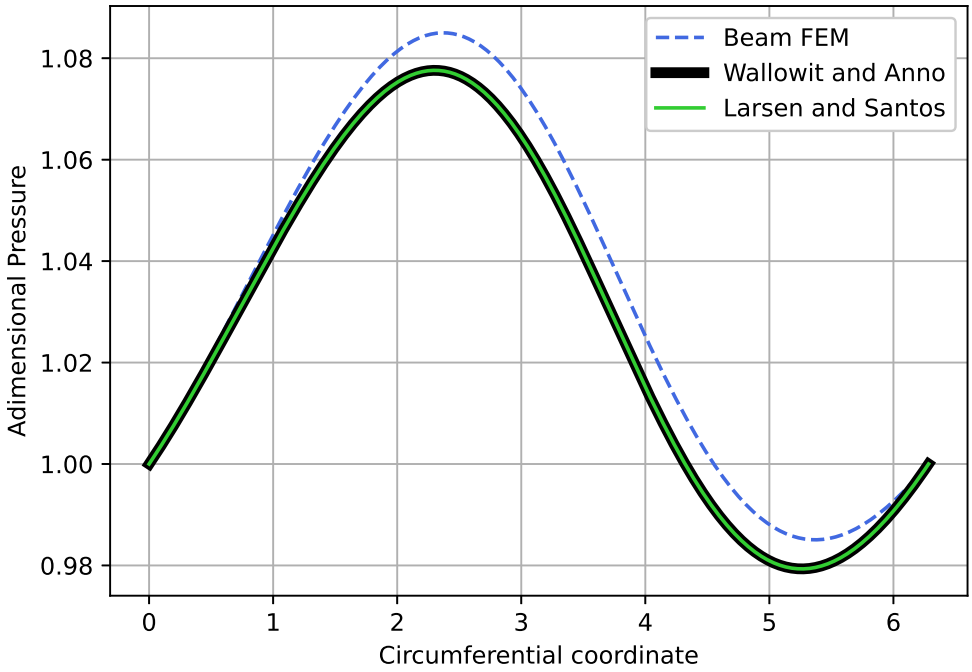

Figure 4.12: Pressure field $\tilde{p}$ with top foil modelling.

For both models, the bump foil is modelled using Wallowit and Anno's model. The difference between the two models lies in the definition of the top foil modelling for the two models. In Larsen and Santos' model, the top foil is modelled by simply including a correction term based on the assumption of a continuous periodic top foil. This correction term is applied to the compliance of the SEFM, which is then used to compute the gap $\tilde{h}$. For the beam FEM top foil modelling, the top foil's deflection under the action of the pressure field is computed, adimensionalised and then finally added to the overall gap $\tilde{h}$.

The loss of circumferential symmetry in the gap field $\tilde{h}$ can be noticed from Figure 4.11. This could be expected as the beam FEM modelling of the top foil assumes that the 360° top foil behaves as a cantilever. The welded end of the foil is considered clamped and stays in its initial position, while the free end is free to move.

If the boundary conditions of the beam FEM modelling are adapted to represent a periodic top foil layer to match the assumption of the Larsen and Santos' model, both models

produce very similar results. These results are shown in Figure 4.13 and Figure 4.14. Hence, both top foil representations can be considered somewhat equivalent, with the exception that the beam FEM modelling allows for the representation of various BCs and thus for a broader analysis range.

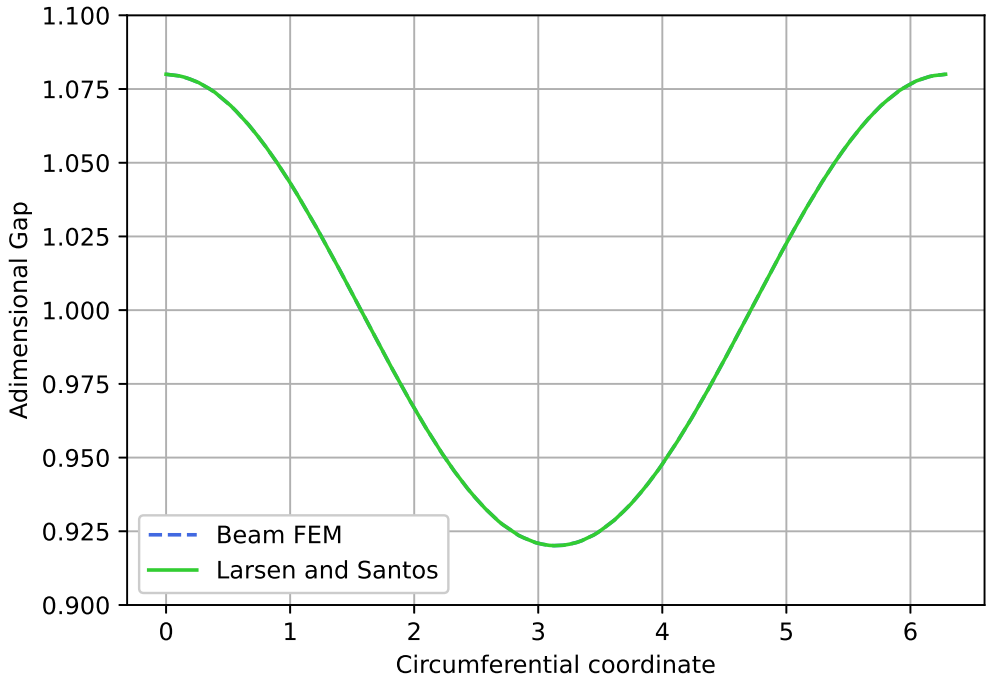

Figure 4.13: Gap field $\tilde{h}$ with top foil periodicity BC.

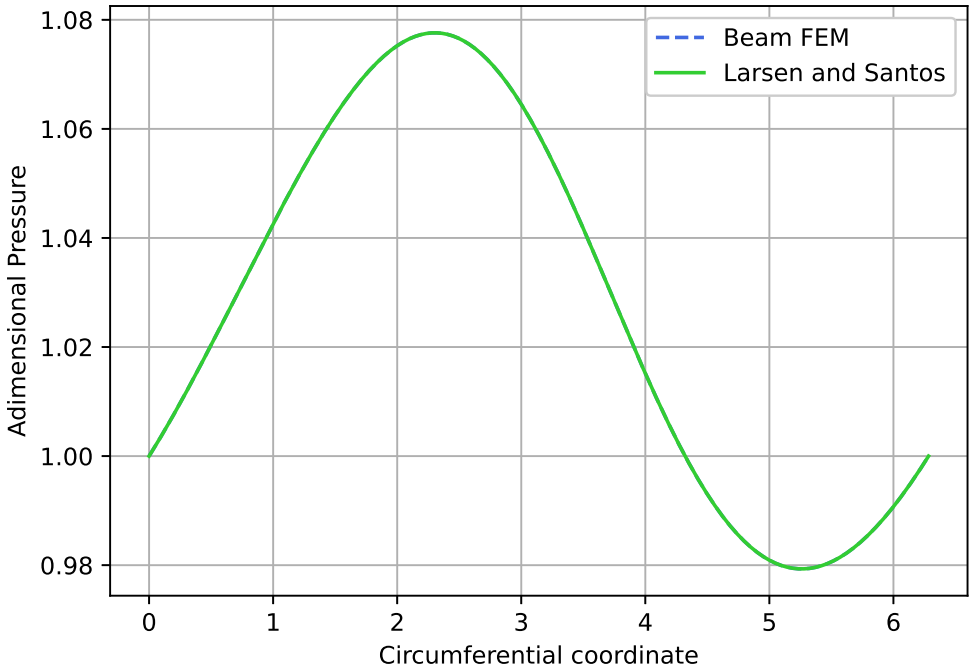

Figure 4.14: Pressure field $\tilde{p}$ with top foil periodicity BC.

4.3 Limitations of Beam FEM Top Foil Modelling

The implementation of this model was done with the purpose of showing the good behaviour of the externalisation of the structural solver and showing that new solvers could be introduced and coupled with ForDGe without any issue. This is especially true for globalised structural models, which would be difficult to implement in ForDGe by direct coupling. Nevertheless, the beam FEM is not the best model for the top foil in terms of accuracy and numerical precision. Moreover, as only steady-state static analysis has been performed, the FEM employs a linear system that could potentially be directly implemented inside of ForDGe, but, once again, future dynamic and transient behaviour analysis will require more complex modelling that cannot be merged inside of ForDGe.

The beam finite element method presents some limitations regarding the top foil of GFBs modelling. Actually, the top foil of a GFB cannot be assumed to be equivalent to

a beam for various reasons. The top foil could be made of layers of different materials for thermal or startup wear protection motivations. These different layers and specific materials could have varying properties during the operation phase. That would be ignored by the beam assumption. Also, some top foils could have more sophisticated geometries not well modelled by the beam hypothesis.

The beam FEM assumes that the load acting on the top foil is distributed, which is not the case regarding the pressure field. The pressure field can vary due to many factors, such as non-linear behaviour from dynamic effects, operation point, temperature and journal rotation speed.

Finally, the contact between the foils is ignored and the friction forces that would also generate some stiffness are also ignored. The coupling between foils is completely neglected and it is assumed that both of their contributions simply add up.

Chapter 5

Conclusion and Perspectives

5.1 Conclusion

This work established a recent review of the current state of the gas foil bearing technology from a design point of view as well as from a modelling point of view. It stands out from this literature review that the technology is in constant evolution and that novel gas foil bearing configurations keep being developed. Every new design is created with the purpose of improving the performances and characteristics of gas foil bearings, such as load capacity, stability, energy dissipation, static and dynamic characteristics.

These novel GFBs come with an increasing order of complexity in their design and thus in their modelling methods, which confirms the necessity for reliable and easy coupling of high order structural and aerodynamic solvers to precisely assess and analyse GFBs' properties. This coupling of high order solvers could not be efficiently implemented internally to ForDGe for each GFB type and modelling technique. This is particularly true for globalised structural solvers.

Then, the implementation of the coupling principle and the iterative process of this coupling to ForDGe as well as the externalisation process of structural solvers from ForDGe and the requirements for any structural solver to be coupled with it were presented.

Finally, the external coupling was validated through comparative analysis with structural solvers implemented both inside and outside of ForDGe. Furthermore, a beam finite element method was implemented to show the good behaviour of ForDGe coupling with a globalised structural solver. Then, it was compared to another GFB top foil model and showed the importance of boundary conditions definition.

5.2 Perspectives

Now that external coupling with ForDGe is functional, further analysis of different GFB configurations and different parameter values can be achieved to deepen the understanding of the technology and to facilitate the industrial applications of GFBs. Thanks to the external coupling interface implemented in the frame of this work, these analyses could be easily carried out with high-order structural solvers to achieve high modelling accuracy. Structural solvers that could be of interest are, of course, complete modelling by finite element analysis, e.g. with curved shell elements or globalised models like the one developed by Arghir and Benchekroun [36] presented in subsection 2.2.2.

Higher order interpolation methods could be introduced instead of the (bi)linear interpolation to measure effects in terms of accuracy and computation time and to try to limit the externalisation induced error.

Lastly, ForDGe could be linked with other solvers and modelling of rotor dynamics to perform dynamic analysis, which requires high multi-physics precision. Naturally, the latter is facilitated by the external coupling of the solvers.

Appendix A

Iordanoff's Formulation Geometric Functions

The geometric functions of Iordanoff's compliance formulation are:

$$I(\theta_b, \mu_f) = \left(A^2 + \frac{1+\mu_f^2}{2}\right)\theta_b - \frac{(1-\mu_f^2)\sin 2\theta_b}{4} \tag{A.1}$$

$$- \frac{\mu_f(\cos 2\theta_b - 1)}{2} - 2A(1 - \cos\theta_b + \mu_f \sin\theta_b), \tag{A.2}$$

$$A = \sin\theta_b + \mu_f \cos\theta_b. \tag{A.3}$$

and

$$J = y_a \left[(\cos\theta_b - 1)A + \frac{\mu_f(1-\cos 2\theta_b)}{4}\right] + (1-y_a)\left(\frac{\theta_b}{2} - \frac{\sin 2\theta_b}{4}\right), \tag{A.4}$$

$$y_a = \frac{-\left(\frac{3\sin 2\theta_b}{4} - \frac{\theta_b}{2} - \sin\theta_b\right)}{2\theta_b \sin\theta_b A - 2\mu_f \sin^2\theta_b + \theta_b - \frac{\sin 2\theta_b}{2}}. \tag{A.5}$$

Iordanoff's formula to compute the compliance both at the free end and at the welded end of a bump foil considers Coulomb friction forces with the bearing sleeve.

Appendix B

Python Interface and Classes Implementation

Hereafter are presented the classes implemented or modified in the context of this work, the Python interface, and a simple test case is described.

- `discretisation`
  - `FDGField.hpp`
  - `FDGSolutionField.cpp/.hpp`
  - `FExternalFieldPython.hpp`
  - `FExternalIJK.cpp/.hpp`
  - `FField.hpp`
- `modules`
  - `ExternalFieldPython.py`
- `swigInterface`
  - `fordge.i`
- `mesh`
  - `[...]`

Each file's purpose is briefly described:

1. `FDGField.hpp`, `FDGSolutionField.cpp/.hpp` and `FField.hpp` have all been implemented to support the update of the solution field and its evaluation each time the residual is computed.

2. `FExternalIJK.cpp/.hpp` is the class that supports the interpolations of the solution field and the structural gap. It is initialized at the solver's creation if ForDGe is coupled with an externalised structural solver.

3. `FExternalFieldPython.hpp` defines to ForDGe the routines of the Python interface.

4. `ExternalFieldPython.py` is the implementation of the Python interface.

5. `fordge.i` is the SWIG file that ensures good communication between ForDGe and the Python interface.

6. Finally, a few modifications have been performed in the `mesh` folder of ForDGe to handle the evaluation of the solution field on the structural solver's mesh.

The procedure to initiate a simple test case employing the external beam FEM and Wallowit and Anno's SEFM formulation for the bump foil takes place as follow:

1. The test case parameters must be defined in the corresponding *.json* file, in which the parameter *top_foil_modelling* must be set equal to *True* to enable the beam FEM modelling.

2. The structural solver's discretisation parameters must also be defined, as well as the modelling choices, i.e. *Model = 'External'* and *Ext_model = 'Wallowit'*.

3. Then, in a test file, such as any `test/gasFoilBearing/ParametricStudyXXX.py`, the Python interface must be initiated by creating the relevant Python object, e.g. *externalIJK = ExternalFieldPython(**params)*.

4. Finally, in the test file, after ForDGe's solver has been created and before it is run, the Python interface object must be set, i.e. its address must be given to ForDGe. The setting routine is implemented in `ForDGe/FSolver.hpp` and can be used in the test case file by the Python instruction *solver.setExternalIJK(externalIJK)*.

Bibliography

[1] P. Samanta, N.C. Murmu, and M.M. Khonsari. "The evolution of foil bearing technology". In: *Tribology International* 135 (2019), pp. 305–323. ISSN: 0301-679X. DOI: https://doi.org/10.1016/j.triboint.2019.03.021. URL: https://www.sciencedirect.com/science/article/pii/S0301679X19301410.

[2] II Walton James F., Hooshang Heshmat, and Michael J. Tomaszewski. "Testing of a Small Turbocharger/Turbojet Sized Simulator Rotor Supported on Foil Bearings". In: *Journal of Engineering for Gas Turbines and Power* 130.3 (Mar. 2008), p. 035001. ISSN: 0742-4795. DOI: 10.1115/1.2830855. URL: https://doi.org/10.1115/1.2830855.

[3] Hooshang Heshmat, Michael Tomaszewski, and James Walton. "GT2005-68404 DEMONSTRATION OF A TURBOJET ENGINE USING AN AIR FOIL BEARING". In: June 2005. DOI: 10.1115/GT2005-68404.

[4] Klusman SA. "Klusman SA. Gas turbine engine, machine and self-aligning foil bearing system US Patent Number9657594B2." In: 2017.

[5] *An Assessment of Gas Foil Bearing Scalability and the Potential Benefits to Civilian Turbofan Engines*. Vol. Volume 1: Aircraft Engine; Ceramics; Coal, Biomass and Alternative Fuels; Education; Electric Power; Manufacturing Materials and Metallurgy. Turbo Expo: Power for Land, Sea, and Air. June 2010, pp. 29–35. DOI: 10.1115/GT2010-22118. URL: https://doi.org/10.1115/GT2010-22118.

[6] P Vleugels et al. "High-speed bearings for micro gas turbines: stability analysis of foil bearings". In: *Journal of Micromechanics and Microengineering* 16.9 (Aug. 2006), S282. DOI: 10.1088/0960-1317/16/9/S16. URL: https://dx.doi.org/10.1088/0960-1317/16/9/S16.

[7] Brian Dykas et al. "Design, Fabrication, and Performance of Foil Gas Thrust Bearings for Microturbomachinery Applications". In: *Journal of Engineering for Gas Turbines and Power* 131.1 (Oct. 2008), p. 012301. ISSN: 0742-4795. DOI: 10.1115/1.2966418. URL: https://doi.org/10.1115/1.2966418.

[8] Yu Hou et al. "Application of Gas Foil Bearings in China". In: *Applied Sciences* 11.13 (2021). ISSN: 2076-3417. DOI: 10.3390/app11136210. URL: https://www.mdpi.com/2076-3417/11/13/6210.

[9] Paweł Pietkiewicz Krzysztof Nalepa and Grzegorz Żywica. "DEVELOPMENT OF THE FOIL BEARING TECHNOLOGY". In: *Technical Sciences* 12 (2009), pp. 230–240.

[10] Jon Steffen Larsen. *Nonlinear Analysis of Rotors Supported by Air Foil Journal Bearings - Theory and Experiments*. PhD thesis. DTU Mechanical Engineering, 2014.

[11] Hooshang Heshmat et al. "Oil-Free Turbocharger Demonstration Paves Way to Gas Turbine Engine Applications". In: Turbo Expo: Power for Land, Sea, and Air Volume 1: Aircraft Engine; Marine; Turbomachinery; Microturbines and Small Turbomachinery (May 2000), V001T04A008. DOI: 10.1115/2000-GT-0620. URL: https://doi.org/10.1115/2000-GT-0620.

[12] Michael Branagan et al. "Compliant Gas Foil Bearings and Analysis Tools". In: *Journal of Engineering for Gas Turbines and Power* 138.5 (Nov. 2015), p. 054001. ISSN: 0742-4795. DOI: 10.1115/1.4031628. URL: https://doi.org/10.1115/1.4031628.

[13] H. Heshmat. "Advancements in the Performance of Aerodynamic Foil Journal Bearings: High Speed and Load Capability". In: *Journal of Tribology* 116.2 (Apr. 1994), pp. 287–294. ISSN: 0742-4787. DOI: 10.1115/1.2927211. URL: https://doi.org/10.1115/1.2927211.

[14] Hou Yu et al. "Numerical study on foil journal bearings with protuberant foil structure". In: *Tribology International* 44.9 (2011), pp. 1061–1070. ISSN: 0301-679X. DOI: https://doi.org/10.1016/j.triboint.2011.04.015. URL: https://www.sciencedirect.com/science/article/pii/S0301679X11001174.

[15] Tianwei Lai et al. "Effects of bearing clearance and supporting stiffness on performances of rotor-bearing system with multi-decked protuberant gas foil journal bearing". In: *Proceedings of the Institution of Mechanical Engineers, Part J: Journal of Engineering Tribology* 228.7 (2014), pp. 780–788. DOI: 10.1177/1350650114531406. URL: https://doi.org/10.1177/1350650114531406.

[16] Zhenni Xu, Changlin Li, and Jianjun Du. "Modeling and static characteristics study of the double-layer bump gas foil bearing". In: *Tribology International* 164 (2021), p. 107202. ISSN: 0301-679X. DOI: https://doi.org/10.1016/j.triboint.2021.107202. URL: https://www.sciencedirect.com/science/article/pii/S0301679X21003509.

[17] Kai Feng, Xueyuan Zhao, and Zhiyang Guo. "Design and structural performance measurements of a novel multi-cantilever foil bearing". In: *Proceedings of the Institution of Mechanical Engineers, Part C: Journal of Mechanical Engineering Science* 229.10 (2015), pp. 1830–1838. DOI: 10.1177/0954406214547529. URL: https://doi.org/10.1177/0954406214547529.

[18] Martins Obaseki, P.T. Elijah, and Peter Alfred. "Design analysis and performance evaluation of a novel Multi-Cantilever Foil Bearing". In: *Nigerian Journal of Technology* 40 (Oct. 2021), pp. 449–460. DOI: 10.4314/njt.v40i3.11.

[19] Signe T. Heinemann et al. "Numerical modelling of compliant foil structure in gas foil bearings: Comparison of four top foil models with and without radial injection". In: *Journal of Sound and Vibration* 547 (2023), p. 117513. ISSN: 0022-460X. DOI: https://doi.org/10.1016/j.jsv.2022.117513. URL: https://www.sciencedirect.com/science/article/pii/S0022460X22006964.

[20] Fangcheng Xu et al. "Vibration characteristics control of hybrid radial gas foil bearing-rotor system: Simulation and experiment". In: *Mechanical Systems and Signal Processing* 198 (2023), p. 110402. ISSN: 0888-3270. DOI: https://doi.org/10.1016/j.ymssp.2023.110402. URL: https://www.sciencedirect.com/science/article/pii/S0888327023003096.

[21] Ju-ho Song and Daejong Kim. "Foil Gas Bearing With Compression Springs: Analyses and Experiments". In: *Journal of Tribology* 129.3 (Mar. 2007), pp. 628–639. ISSN: 0742-4787. DOI: 10.1115/1.2736455. URL: https://doi.org/10.1115/1.2736455.

[22] Kai Feng et al. "A novel gas foil bearing with negative Poisson's ratio structure and embedded damping materials: Numerical and experimental investigations". In: *Mechanical Systems and Signal Processing* 198 (2023), p. 110419. ISSN: 0888-3270. DOI: https://doi.org/10.1016/j.ymssp.2023.110419. URL: https://www.sciencedirect.com/science/article/pii/S0888327023003278.

[23] Chuanbing Zhang et al. "Investigations on bearing performances of metal rubber-bump foil gas journal bearing with three structure pads integrating stiffness and damping". In: *Tribology International* 188 (2023), p. 108816. ISSN: 0301-679X. DOI: https://doi.org/10.1016/j.triboint.2023.108816. URL: https://www.sciencedirect.com/science/article/pii/S0301679X23006047.

[24] Robert J Bruckner. "Performance of simple gas foil thrust bearings in air". In: *Supercritical CO2 Power Cycle Symposium*. E-18016. 2012.

[25] Zhenni Xu et al. "Load-carrying characteristics of bump-type gas foil thrust bearings". In: *International Journal of Mechanical Sciences* 244 (2023), p. 108080. ISSN: 0020-7403. DOI: https://doi.org/10.1016/j.ijmecsci.2022.108080. URL: https://www.sciencedirect.com/science/article/pii/S0020740322009584.

[26] Alshikh Saleh Ammar. *Modelling of Gas Foil Bearing with a high order Discontinuous Galerkin Method*. University of Liège, 2022.

[27] H. Heshmat, J. A. Walowit, and O. Pinkus. "Analysis of Gas-Lubricated Foil Journal Bearings". In: *Journal of Lubrication Technology* 105.4 (Oct. 1983), pp. 647–655. ISSN: 0022-2305. DOI: 10.1115/1.3254697. URL: https://doi.org/10.1115/1.3254697.

[28] Marc Carpino, Lynn A. Medvetz, and Jih-Ping Peng. "Effects of Membrane Stresses in the Prediction of Foil Bearing Performance©". In: *Tribology Transactions* 37.1 (1994), pp. 43–50. DOI: 10.1080/10402009408983264. URL: https://doi.org/10.1080/10402009408983264.

[29] I. Iordanoff. "Maximum Load Capacity Profiles for Gas Thrust Bearings Working Under High Compressibility Number Conditions". In: *Journal of Tribology* 120.3 (July 1998), pp. 571–576. ISSN: 0742-4787. DOI: 10.1115/1.2834589. URL: https://doi.org/10.1115/1.2834589.

[30] I. Iordanoff. "Analysis of an Aerodynamic Compliant Foil Thrust Bearing: Method for a Rapid Design". In: *Journal of Tribology* 121.4 (Oct. 1999), pp. 816–822. ISSN: 0742-4787. DOI: 10.1115/1.2834140. URL: https://doi.org/10.1115/1.2834140.

[31] C.-P. Roger Ku and H. Heshmat. "Compliant Foil Bearing Structural Stiffness Analysis: Part I—Theoretical Model Including Strip and Variable Bump Foil Geometry". In: *Journal of Tribology* 114.2 (Apr. 1992), pp. 394–400. ISSN: 0742-4787. DOI: 10.1115/1.2920898. URL: https://doi.org/10.1115/1.2920898.

[32] C.-P. Roger Ku and Hooshang Heshmat. "Compliant Foil Bearing Structural Stiffness Analysis—Part II: Experimental Investigation". In: *Journal of Tribology* 115.3 (July 1993), pp. 364–369. ISSN: 0742-4787. DOI: 10.1115/1.2921644. URL: https://doi.org/10.1115/1.2921644.

[33] Fangcheng Xu, Jianhua Chu, and Long Sha. "Air foil thrust bearings with top foil sagging: Theoretical predictions and experiments". In: *Tribology International* 177 (2023), p. 107995. ISSN: 0301-679X. DOI: https://doi.org/10.1016/j.triboint.2022.107995. URL: https://www.sciencedirect.com/science/article/pii/S0301679X22005667.

[34] Sébastien Le Lez, Mihaï Arghir, and Jean Frene. "A New Bump-Type Foil Bearing Structure Analytical Model". In: *Journal of Engineering for Gas Turbines and Power* 129.4 (Apr. 2007), pp. 1047–1057. ISSN: 0742-4795. DOI: 10.1115/1.2747638. URL: https://doi.org/10.1115/1.2747638.

[35] Aurelian Fatu and Mihai Arghir. "Numerical Analysis of the Impact of Manufacturing Errors on the Structural Stiffness of Foil Bearings". In: *Journal of Engineering for Gas Turbines and Power* 140.4 (Oct. 2017), p. 041506. ISSN: 0742-4795. DOI: 10.1115/1.4038042. URL: https://doi.org/10.1115/1.4038042.

[36] Mihai Arghir and Omar Benchekroun. "A simplified structural model of bump-type foil bearings based on contact mechanics including gaps and friction". In: *Tribology International* 134 (2019), pp. 129–144. ISSN: 0301-679X. DOI: https://doi.org/10.1016/j.triboint.2019.01.038. URL: https://www.sciencedirect.com/science/article/pii/S0301679X19300465.

[37] Chenfei Wang, Xiaoli Wang, and Yanqiang Hu. "Investigation on start-up performance of gas foil bearing considering wear topography evolution of non-Gaussian surface". In: *Tribology International* 177 (2023), p. 108003. ISSN: 0301-679X. DOI: https://doi.org/10.1016/j.triboint.2022.108003. URL: https://www.sciencedirect.com/science/article/pii/S0301679X22005746.

[38] Koen Hillewaert. *The discontinuous Galerkin method A short intro to theory and practical implementation*. Mar. 2023.

[39] Sebastian von Osmanski and Ilmar F. Santos. "Gas foil bearings with radial injection: Multi-domain stability analysis and unbalance response". In: *Journal of Sound and Vibration* 508 (2021), p. 116177. ISSN: 0022-460X. DOI: https://doi.org/10.1016/j.jsv.2021.116177. URL: https://www.sciencedirect.com/science/article/pii/S0022460X21002492.

[40] Koen Hillewaert. *Development of the discontinuous Galerkin method for high-resolution, large scale CFD and acoustics in industrial geometries*. Presses univ. de Louvain, 2013.

[41] Arnold Sommerfeld. "Zur Theorie der Schmiermittelreibung". In: *Archiv für Elektrotechnik* 3.1 (1914), pp. 1–5.